**Catarina Fortunato Martins**

Licenciada em Ciências Forenses e Criminais

# Laser ablation of tumour cells via precision nanomedicine

Dissertação para Obtenção do Grau de Mestre em

Biotecnologia

Orientador:

Prof. Doutor Pedro Miguel Ribeiro Viana Baptista, Professor Catedrático, Faculdade de Ciências e Tecnologia da Universidade Nova de Lisboa

Júri

Presidente: Prof. Carlos Alberto Gomes Salgueiro, FCT

Arguentes: Prof. João Carlos Lima, FCT

Data: 22/4/21

FACULDADE DE CIÊNCIAS E TECNOLOGIA
UNIVERSIDADE NOVA DE LISBOA

**Laser ablation of tumour cells via precision nanomedicine**

*Dedicado aos meus pais e ao meu amor…*

# Agradecimentos

A execução desta tese de mestrado só foi possível com a ajuda de várias pessoas, incluindo todo o trabalho, erro e tentativa que mesmo não estando registado sem eles este trabalho não faria sentido.

Tenho de agradecer do fundo do meu coração ao meu orientador Prof. Pedro Baptista, por me ajudar nesta fase da minha vida, auxiliando-me a ultrapassar obstáculos, mas acima de tudo a formar uma pessoa com um carácter do qual me orgulho bastante no final desta etapa. A energia, os puxões e as discussões auxiliaram-me a formar um pensamento crítico, a ter autonomia assim como pela paixão/motivação que me transmitiu. Deixo aqui uma mensagem que espero que fique registada para todo o sempre:

“Don’t wish it was easier, wish you were better. Don't wish for fewer problems, wish for more skills. Do not wish for fewer challenges, wish for more wisdom. The major value in life is not what you get. The major value in life is what you become. Success is not to be pursued; it is to be attracted by the person you become.” – Jim Rohn

Obrigada aos meus amigos/as que me acompanharam durante esta jornada, David por todo o apoio e ajuda; Daniela, Beatriz e Inês por todas as gargalhadas e conversas divertidas e animo; Catarina e Luís por todo o esforço que fizeram a ajudar todos os alunos de mestrado; a minha santa Margarida por me aturar; Pedrosa e Lourenço por me ajudarem sempre que eu precisava e ao Rafael o aluno de licenciatura que tive o enorme prazer de orientar e que também me ajudou no decurso da minha tese de mestrado. Para além dos que referi, queria agradecer aos amigos e familiares que ao longo destes meses tiveram de aturar o meu “stress”, muito obrigada a todos por tudo.

Talvez não devesse, mas em último agradeço aos grandes pilares da minha vida, os meus pais e o meu amor. Sinto que tenho evoluído muito ao longo destes anos, num declive positivo, formando-me com um carácter e valores do qual me orgulho imenso. Obrigada por terem feito de mim aquilo que sou, por me mimarem e ensinarem a crescer. Para os meus pilares deixo também uma mensagem muito querida e que espero que fique marcada para toda a eternidade:

“The only transformer, the only alchemist who changes everything into gold, is love. The only antidote against death, age, vulgar life, is love." - Anaïs Nin

継続は力なり。 (Keizoku wa chikara nari) Literally: Continuance is power/strength.

# Resumo

O cancro é uma doença complexa que afeta a multiplicação das células, sendo uma das principais causas de mortalidade em todo o mundo. Embora existam vários tipos de terapias oncológicas disponíveis, a mais usada para tratar o cancro é a cirurgia e a quimioterapia, ambas com efeitos secundários indesejados e limitados ao tipo de cancro. A nano medicina é o campo da ciência e da tecnologia, que utiliza sistemas à escala nano para o diagnóstico, tratamento ou prevenção de uma doença. As nanopartículas de ouro (AuNPs) são utilizadas em diversas aplicações, devido às suas propriedades como a biocompatibilidade, relação superfície-volume elevada e facilidade de funcionalização. As AuNPs são usadas principalmente em fototerapia, uma vez que a radiação irá desencadear uma conversão foto térmica, destruindo as células cancerígenas e por sua vez reduzindo o volume do tumor. A terapia genética tem surgido como uma excelente abordagem para a terapia oncológica, utilizando oncogenes ou supressores de tumores. *c-MYC* é um dos oncogenes mais estudados, cuja expressão é desregulamentada em vários cancros, estando envolvido na proliferação, crescimento e metabolismo celular. Deste modo, foi sugerida uma terapia combinada, explorando as AuNPs como sistemas de "theranostic", entre a terapia genética e fototerapia. Os resultados obtidos da sinergia de ambas as terapias puderam indicar que a hipertermia aumenta a permeabilidade celular, aumentando assim o silenciamento genético do *c-MYC* em quase 70%.

**Palavras-chave:** Cancro; Terapia genética; Fototerapia; Nanotecnologia; Nanopartículas de ouro; *c-MYC*.

# Abstract

Cancer is defined as a complex set of diseases that affect the multiplication of cells, being one of the leading causes of mortality worldwide. Although several types of cancer therapies are available, the most used to treat cancer are surgery and chemotherapy, both with several side effects and limited to certain types of cancer. Nanomedicine is the science and technology field that uses nanoscale systems to diagnose, treat, or prevent a disease. Gold nanoparticles (AuNPs) are highly used in biomedical applications due to their physical-chemical properties like biocompatibility, high surface-area-to-volume ratio, and ease of functionalization. AuNPs are mainly used in photothermal therapy, since the radiation will trigger a thermal photo conversion, destroying cancer cells thus reducing the tumour volume. Gene therapy has emerged as an excellent approach to cancer therapy, using genes to treat a disease using oncogenes or tumour suppressors. *c-MYC* is an oncogene widely studied, whose expression is deregulated in various cancers, being involved in cell proliferation, growth, and metabolism. Thus, it was suggested a combinatory therapy, exploring the AuNPs as "theranostic" systems, between gene therapy and photothermal therapy. The results achieved of the synergy of both therapies indicate that hyperthermia enhances the cell permeability, thus increasing the gene silencing of the *c-MYC* by almost 70%.

**Keywords:** Cancer; Gene therapy; Phototherapy; Nanotechnology; Gold Nanoparticles; *c-MYC*.

# List of Publications

Included in this thesis:

Ferreira, D.; Fontinha, D.; **Martins, C**.; Pires, D.; Fernandes, A.R.; Baptista, P.V. Gold Nanoparticles for Vectorization of Nucleic Acids for Cancer Therapeutics. *Molecules* **2020**, *25*, 3489.

# List of Abbreviations

ASO – Antisense oligonucleotides

ATP – Adenosine triphosphate

AuNPs – Gold nanoparticles

*c-MYC* – Proto-oncogene

cDNA – Complementary DNA

CNT – Carbon Nanotubes

Csca/Cabs – Quotient between the Cross-section scattering and absorption

DLS – Dynamic light scattering

DMEM – Dulbecco´s Modified Eagle Medium

EPR – Enhanced Permeability and Retention

FBS – Fetal Bovine Serum

HSPs – Heat Shock Proteins

ICP-AES – Inductively Coupled Plasma-Atomic Emission Spectroscopy

IFP – Interstitial Fluid Pressure

IR – Infrared

MDR – Multiple Drug Resistance

MHC molecule – Major histocompatibility complex molecule

mRNA – Messenger RNA

MTS assay – (5-(3-carboxymethoxyphenyl)-2-(4,5-dimethyl-thiazolyl)-3-(4-sulfophenyl) tetrazolium, inner salt assay)

MYC protein –MYC Proto-Oncogene, bHLH Transcription Factor

NIR – Near-Infrared

NK cells – Natural killer cells

NPs – Nanoparticles

PBS – Phosphate Buffer Saline

PCR – Polymerase Chain Reaction

PDT – Photodynamic Therapy

PEG – Polyethylene glycol

PTT – Photothermal Therapy

RISC – RNA-induced silencing complex

ROS – Reactive oxygen species

RT-qPCR – Real-time quantitative polymerase chain reaction

SDS – Sodium Dodecyl Sulphate

siRNA – small interfering RNA

SPR – Surface Plasmon Resonance

ssDNA – Single-Stranded DNA

STR – Short Tandem Repeat

UV – Ultraviolet

UV-Vis – Ultraviolet-visible

Vis – Visible

ZP – Zeta Potential

# Index

# List of Figures

# List of tables

# 1 Introduction

This chapter aims to present the key concepts used in this thesis. Here, it will be introduced the topic of cancer as well as an overview of the different types of cancer therapies; the concepts of nanotechnology and nanomedicine; the use of nanoparticles as carriers for therapy; laser ablation in medicine; a combined approach in cancer therapy; finishing with primary objectives and framework of the present study.

## 1.1 Cancer

Cancer is known to be one of the leading causes of death worldwide, remaining a medical challenge due to the complex combination of various diseases [1].

Cancer is characterized by the unlimited division and survival of abnormal cells. Cancer cells hold special features essential for tumour growth, such as the invasion-metastasis mechanism and the ability to induce angiogenesis. This complexity is intimately related to the genome's dynamic transformation, caused by mutations or epigenetic modifications in specific genes that lead to abnormal growth and loss of cell differentiation [2]. The formation of metastases is a product of cell-biological events, formally referred to as invasion-metastasis cascades. During the metastatic progression, the tumour cells escape their primary sites of growth with a local invasion in adjacent tissue, migrate to new sites, and form new secondary tumours by escaping from the blood or lymph vessels [3]–[5].

Angiogenesis, the formation of new blood and lymph vessels, is a crucial step in metastasis since it enhances the entry of tumour cells into the blood and lymphatic circulation system. The enhanced cellular uptake is possible due to the new vessels formed being highly permeable, composed of small basement membrane with fewer intercellular functional complexes than normal mature vessels [6], [7].

Another important mechanism that many cancers develop is the immune response evasion. The tumour cells may evade the immune system response by evading the immune cell detection or by inhibiting the anti-tumour immune response. The most common tumour escape mechanisms are by downregulation of the MHC class I molecules expression or by preventing the recruitment of dendritic cells or effector T cells into the tumour. It is essential to notice that the tumour microenvironment also influences the T cells and NK cells' functions, suppressing the anti-tumour immune response [8].

### 1.1.1 Colorectal cancer

The colon and rectum (colorectum) are part of the large intestine, the final part of the gastrointestinal (GI) system (figure 1.1). When the abnormal growth of cells occurs in the colon or rectum, it is called colorectal cancer (CRC). CRC is characterized as a malignant, invasive, and solid tumour formed in the epithelial layer of the large intestine wall [9], [10]. CRC factors risks are usually associated with the increase in average population age, sedentary lifestyle, and environmental risk factors like lack of physical activity, smoking, and high meat and alcohol consumption [11].

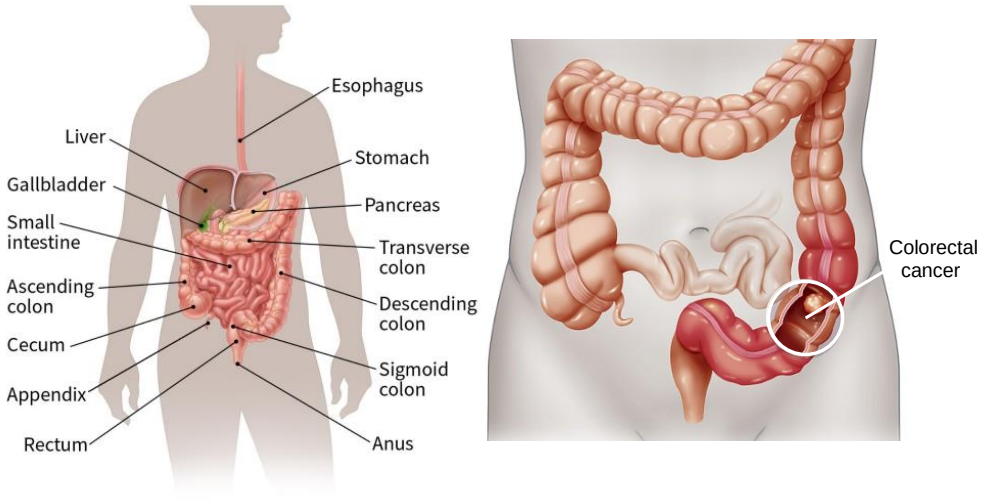


Figure 1.1: Illustration of the colon and rectum, which is part of the digestive system, also called the gastrointestinal system. On the right, a more detailed view regarding the location of colorectal cancer [12].

CRC represents an ideal cancer model to investigate since the tumour progression is based on a series of genetic alterations translated to well-defined histopathological changes, the so-called adenoma-carcinoma sequence. The adenoma-carcinoma sequence describes the abnormal growth of polypoid lesions in the intestine (adenoma). Although it is common to have some lesions in the large intestine, these adenomas are associated with the increased size and dysplasia of the epithelium. The adenoma-carcinoma sequence is mostly related to genetic alterations, due to the activation of oncogenes (e.g., *c-MYC*) and inactivation of tumour suppressor genes (e.g., *p53*) [11].

Statistics show in the diagram of figure 1.2, that this type of cancer has high rates of mortality and incidences, worldwide. Compared with Portugal cancer cases, in figure 1.3, it is possible to observe that CRC is also very predominant, having a high incidence rate.

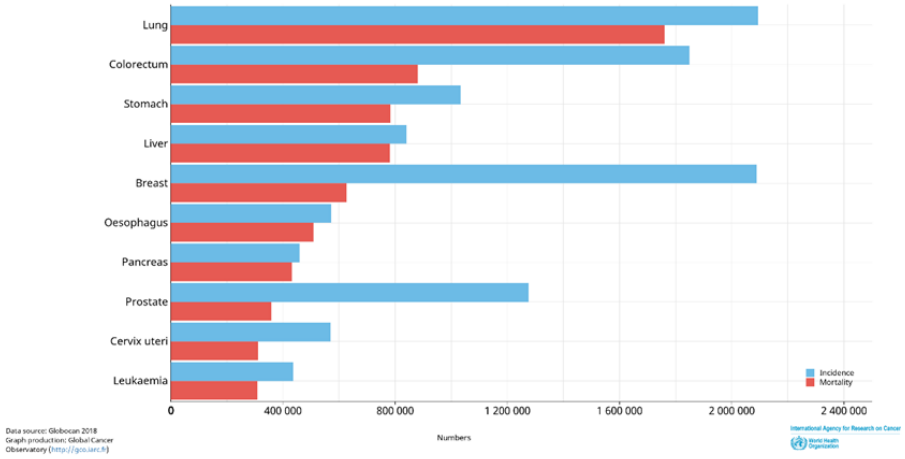


Figure 1.2: Cancer statistics with the number of incident cases and deaths worldwide, for both sexes and ages [1]. The statistics show a large incidence of lung, colorectum, and breast cancer. However, colorectum cancer persists as one of the cancer types with high rates of incidence and mortality worldwide.

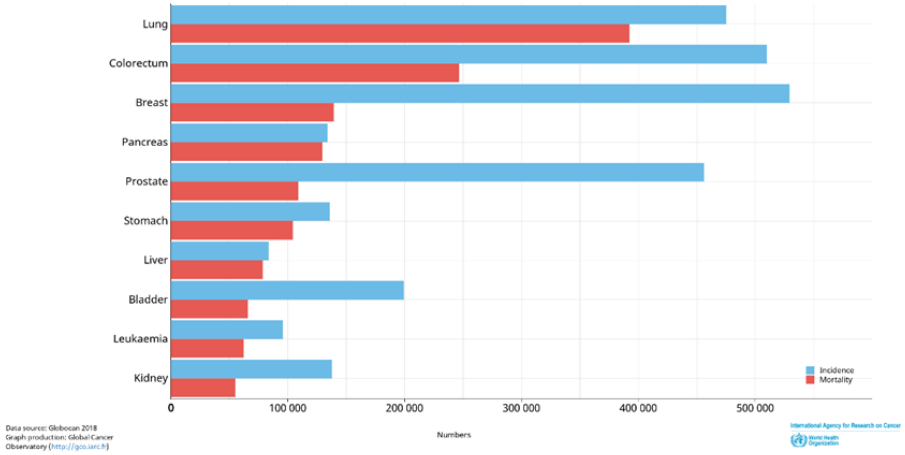


Figure 1.3: Cancer statistics with the number of incident cases and deaths in Portugal, for both sexes and ages [1]. Portugal presents some similar cancer profile statistics, where colorectum cancer remains with high rates of both incidence and mortality.

### 1.1.2 Cancer therapy

There are different cancer therapies, depending on the type of cancer and how advanced it is. Each type of therapy has a unique agent of action and its pros and cons, which are broadly highlighted in table 1.1 [13]–[15].

Table 1.1: Representation of different types of cancer therapies with their respective characteristics [16].

| Type of therapy | Agent of action | Advantages | Disadvantages |
|---|---|---|---|
| **Chemotherapy** | Chemotherapy is a type of anti-cancer drug treatment. | This type of treatment is also called systemic treatment since it acts throughout the body patient. | Different drugs cause different side effects, plus their effect depends on the type of cancer, tissue, and patients' general health. |
| **Surgery** | Surgery is based on the removal of the malign tissue from the body. | This treatment is the primary medical procedure used for solid localized tumours (e.g., breast cancer). | Invasive and destructive medical procedure. It is limited to the type of the tumour since it cannot be applied to certain types of cancer (e.g., lymphoma). |
| **Radiotherapy** | Radiotherapy is based on ionizing radiation of high energy (e.g., x-rays). | Uses high doses of radiation to kill cells, control, and shrink tumours. | This medical procedure is destructive since it affects normal cells, causing several side effects in the patient body. |
| **Immunotherapy** | Immunotherapy is a type of drug treatment that uses the body's own immune system to fight cancer (e.g., monoclonal antibodies and T cells). | Targeted and personalized therapy. | This treatment has limited efficacy and may cause side effects. |
| **Hormone therapy** | Hormone therapy is a treatment that focuses on the block or lowers the number of hormones in the body to slow down or stop the growth of cancer. | Mostly used for hormone-sensitive/dependent cancer (e.g., breast or prostate cancer). | It depends on the type of hormone therapy, the dose, and how long the medication is taken (long-term effects on the immune system). |
| **Gene therapy** | Gene therapy is a type of treatment based on the therapeutic delivery of nucleic acids into a patient's cells to treat a disease. | Gene therapy can be used in combinatory therapies such as chemotherapy or radiotherapy to increase the specificity and efficiency of the treatment. | It could trigger unwanted immune system reactions. |

## 1.2 Nanotechnology and Nanomedicine

Nanoscience is an interdisciplinary concept that cuts across all vertical sciences and engineering disciplines, involving the study of materials that exhibit unique properties and functionalities at small dimensions. The application of nanoscience to practical devices is called nanotechnology. Nanotechnology consists of the design, characterization, production, and application of structures, devices, or systems at a nanoscale ($10^{-9}$ m) [17]–[19].

Nanomaterials have unique characteristics compared to bulk materials, having novel optical, chemical, and mechanical properties useful for diagnosing and treating diseases such as cancer. As such, the concept of nanomedicine was created, with the use of nanomaterials as smart components for diagnostic or supporting cooperative therapies. Nanomedicine is a potentially efficient method to treat cancer, being a possible solution to the main problems cancer therapies face like the low specificity, rapid drug clearance, biodegradation, and limiting targeting [20], [21].

The use of these nanomaterials and nanoparticles (NPs) in medicine to formulate drugs or new therapeutic agents, has created many physical and biological advantages translated into improved therapeutic efficiency and reduced toxicity. Recently their use has been expanded towards the diagnostic field, where these nanomaterials can be designed as contrast agents. Another aspect is the multifunctional use of NPs for targeted therapies in cancer, to bind specifically or transport biomolecules on the target site, complemented with image tools. This allows a combined therapeutic and diagnosis effect in a complete system referred to as theranostic (figure 1.4). The main goal of the theranostic system is to have the ability to diagnose and monitor the diseased tissue, combined with targeted drug delivery in a controllable manner [18], [21], [22].

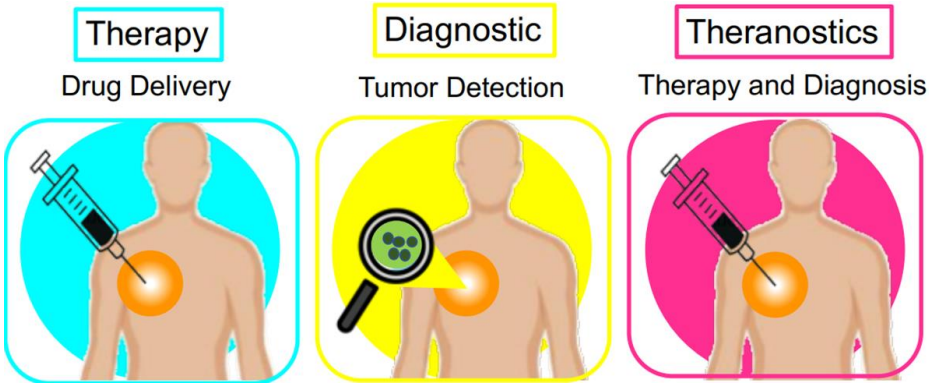


Figure 1.4: Representation of theranostic. Theranostic is the combination of diagnostic (represented with bio-imaging tools) and therapy (represented with drug delivery tools).

### 1.2.1 Nanoparticles as nanocarriers in cancer therapy

NPs size, type, shape, composition, surface charge, and biocompatibility will dictate their behaviour *in vivo* as well as their therapeutic effect. For the design of an efficient nanocarrier, it is crucial to have: precise control over (a) biodistribution; (b) targeting; (c) *in vivo* stability; (d) circulation kinetics; and (e) drug release mechanisms [23]. In terms of the NPs size, it is known that it affects the particle circulation in blood or lymph vessels. As such, NPs with a small diameter are quickly eliminated from the body, excreted by the kidneys, lowering their circulation time. While NPs with a larger diameter than the blood capillaries cannot circulate in the body, being trapped in the capillary bed [23], [24]. Figure 1.5 exemplifies the most important NPs properties for therapeutic applications.

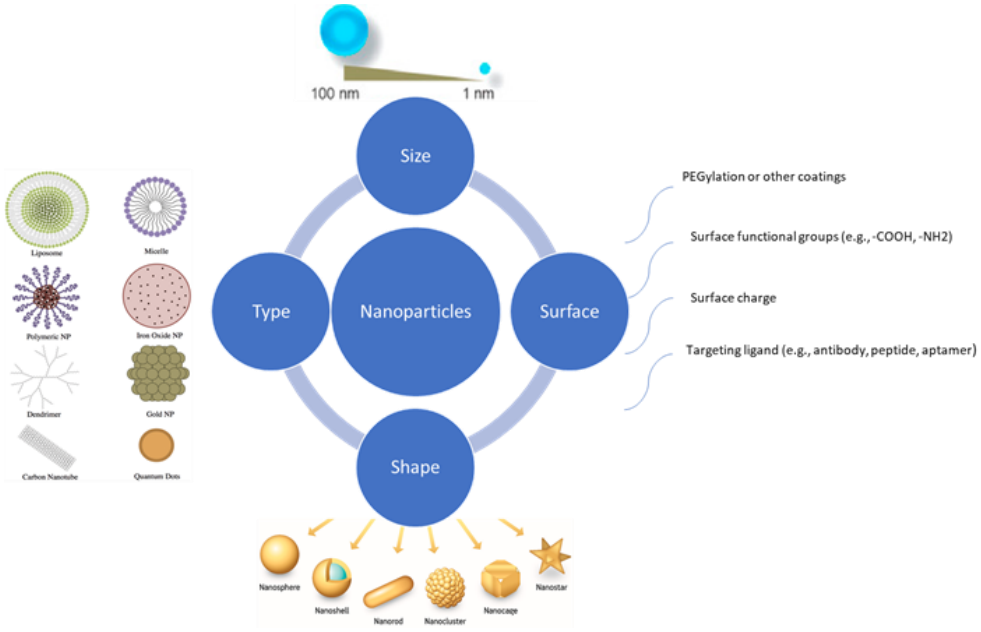


Figure 1.5: Exemplification of NPs categorized according to their type, size, surface, and shape. Adapted from T. Sun, Y. S. Zhang, B. Pang, D. C. Hyun, M. Yang, and Y. Xia, "Engineered Nanoparticles for Drug Delivery in Cancer Therapy," Angew. Chemie Int. Ed., vol. 53, no. 46, pp. 12320–12364, Nov. 2014.

There are different types of NPs; as such, table 1.2 summarizes several NPs with their principal characteristic, applications, and limitations [25].

Table 1.2: Representation of the different types of NPs in cancer therapy and their respective applications and limitations.

| Type of NP | Characteristics | Application | Limitations |
|---|---|---|---|
| **Dendrimer** [26], [27] | Dendrimers are small (1–15nm) branched or tree-like monodisperse polymeric NPs. Dendrimers have high water solubility, high loading capacity, and low immunogenicity. | These dendritic polymers are analogous to protein and are easily functionalized. | Their synthesis is quite time-consuming, plus it has issues in toxicity, incorporation, and drug release. |
| **Liposome** [28], [29] | Nanostructures are made of amphiphilic molecules, like polymers or lipids. These nanostructures present biocompatibility, low immunogenicity, enhanced cellular uptake, and biodegradable nature. | Liposomes are a versatile nanocarrier, with the ability to load amphiphilic drugs due to their hydrophobic tail and hydrophilic head region. | These are quite unstable NPs, with rapid degradation, fast clearance from the body, and present phospholipids' oxidation. |
| **Polymeric** [30], [31] | The polymer can be natural (proteins and polypeptides) or artificial/synthetic polymer. These polymeric NPs have high biocompatibility and biodegradation. | Polymeric NPs can combine both therapy and imaging (theranostic), enhancing the target treatment's specificity. | These NPs have low transfection efficiency and undesirable cytotoxicity. |
| **Carbon-based NP** [32], [33] | Carbon-based NPs have been explored for biomedical applications. These are biocompatible, biodegradable, and have unique mechanical and optical properties. | They are mostly used for imaging and drug delivery applications. | Cytotoxicity. |
| **Quantum dots** [34], [35] | Quantum dots are luminescent nanoprobes that present high photostability, being very resistant to photobleaching. | Used in imaging, detection, and targeting. | High toxicity due to the CdSe (the metallic core of the NPs). |
| **Gold Nanoparticle (AuNP)** [36], [37] | AuNPs are composed of a metallic core, presenting unique optical and physical-chemical properties. | AuNPs have been primarily used for labelling applications; however, they are also used in combinatory therapy. | Effect of size on toxicity, efficacy, biodistribution, and physiological response. |
| **Magnetic NP** [38], [39] | Magnetic particles may be used to selectively attach, manipulate, or transport targeted species to the desired location under the influence of an external magnetic field. | These NPs are widely used as contrast agents in MRI (Magnetic Resonance Imaging). | These NPs have limitations regarding the range of magnetic influence and chemical resistance. |

### 1.2.2 Drug delivery and targeting

NPs can reach the target tissue by passive and active cell targeting. The passive targeting is mainly due to the Enhanced Permeability and Retention (EPR) effect where by taking advantage of the tumour microenvironment vasculature, allows larger particles to pass through the endothelium [23], [40] The enhanced permeability occurs due to the accelerated vascularization, in response to the nutritional needs required for cancer tissues' proliferative ability. This biological event translates into gaps in the surrounding vessels, leading to extravasation of NPs into cancer cells interstitial fluid, whose retention is ensured by the characteristic absence of lymphatic drainage [40]. The drawback of the EPR effect is the inhomogeneity in the interstitial holes, which affects the penetration and distribution of NPs within the tumour [30], [41], [42].

Active cell targeting, also known as the ligand-mediated target approach, is achieved by the surface functionalization of nanocarriers with targeted portions that provide selective recognition of different receptors or overexpressed antigens in cancer cells. As such, the therapeutic agent performs in a more specific and selective manner, increasing their therapeutic efficacy [22], [23], [43]. Ligands can be proteins (antibodies or fragments), nucleic acids (DNA or RNA), or small molecules (peptides, aptamer, vitamins, glycoprotein, or carbohydrates such as lectins). A classic example of active targeting is lectin-carbohydrate, a protein receptor present on the cell surface, used in antiproliferative activities by inhibiting the metastatic spread and tumour growth [30], [41], [43]. Figure 1.6 identifies the types of drug delivery.

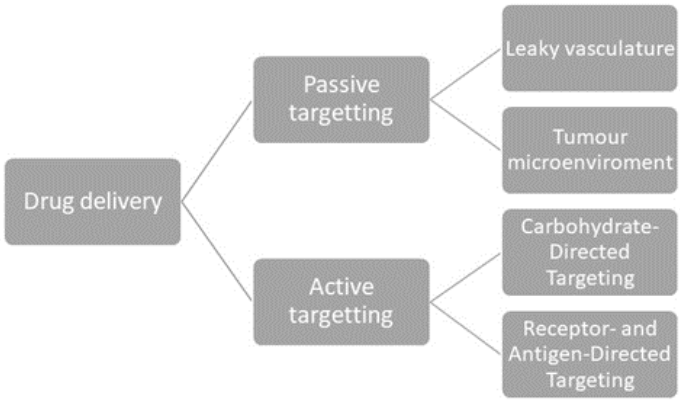


Figure 1.6: Mechanism of NP drug delivery via two main mechanisms—passive and active targeting. Adapted from R. Sinha, G. J. Kim, S. Nie, and D. M. Shin, "Nanotechnology in cancer therapeutics: bioconjugated nanoparticles for drug delivery," Mol. Cancer Ther., vol. 5, no. 8, pp. 1909 LP – 1917, Aug. 2006.

### 1.2.3 Cellular internalization of NP

Cellular uptake has a vital role in the therapy response, as many drugs are directed towards intracellular targets [44]. The NPs enters the cell through endocytose vesicles, mainly mediated by a network of cellular endosomes in conjunction with the Golgi complex, endoplasmic reticulum, and lysosomes [45]–[47]. The two main pathways of endocytic are phagocytosis and pinocytosis, where NPs are mostly internalized by phagocytosis. While pinocytosis is a process by which liquid droplets are ingested by living cells, phagocytosis is a common mechanism in cells with phagocytic capacity (macrophages, neutrophils, monocytes, and dendritic cells) to internalize particles (e.g., NPs) [47], [48].

Depending on the NPs size, shape, and functionalization the cellular internalization can be either receptor-mediated endocytosis or non-specific receptor-independent endocytosis. The most effective NP uptake mechanism is the receptor-mediated endocytosis, where molecules (ligands) surrounding the particle surface bind to the receptors expressed on the cell membrane. The receptors over the cell membrane are collected at the invagination site by surface diffusion, permitting the endocytosis [49].

### 1.2.4 AuNP application in cancer therapy

Nanomedicine focuses on improving traditional medicines by incorporating biocompatible nanocarriers, such as NPs. Among the different NPs the AuNPs are the most studied and used in biomedical applications. AuNPs are multifunctional agents, used for both diagnosis and therapeutic tools, due to their unique physical-chemical properties like a high surface area to volume ratio, SPR, surface chemistry, and stable nature [50].

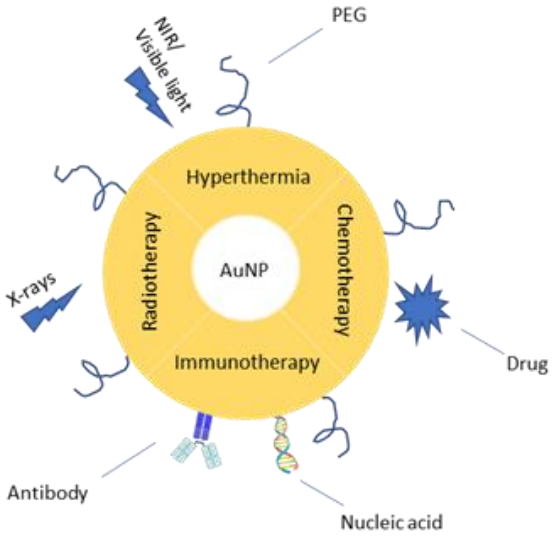


Figure 1.7: Representation of an AuNP and the different cancer therapy applications. AuNPs are characterized by being versatile, with the possibility of having different conjugates on their surface, as showed in the figure, having several applications on different therapies. Adapted from R. Mendes, A. R. Fernandes, and P. V. Baptista, "Gold nanoparticle approach to the selective delivery of gene silencing in cancer-The case for combined delivery?" Genes (Basel)., vol. 8, no. 3, 2017.

AuNPs have unique optical properties at the nanoscale, like the Surface Plasmon Resonance (SPR) effect, frequently used in biological detections. The SPR effect consists of a collective resonant oscillation of conduction electrons, excited by the electromagnetic field of the light [20], [36], [54]. The SPR is quite sensitive to the composition, size, shape, and environment (dielectric properties) of the AuNPs. The UV-Vis spectrum of an AuNP solution with a diameter around 14 nm, generally shows a strong absorption band with a maximum at 520 nm [36], [53], [55]–[57]. If there is an aggregation of the NPs, the spectrum changes, resulting in a spectrum shifting to higher wavelengths [51]. As a result, the SPR can be used to measure biomolecular interactions in real-time with high sensitivity and with cost-effective methods for biorecognition and detection [52], [53].

The biocompatibility of the AuNP is a crucial factor to consider before clinical applications. When the NPs are internalized by the cells, proteins present in the physiological environment form a coating called "corona" on the surface of the NPs, resulting in an NP-protein complex. This complex, formed due to the immune response, influences the NPs properties and the therapeutic effect desired in the treatment [42], [58].

To prevent immune recognition, the NPs are commonly functionalized with PEG, a biocompatible polymer widely used in several biomedical areas. PEGylation is characterized by the process where the NPs surface is functionalized with PEG. This process

“hides” the NPs, by masking their surface with a hydrophilic layer, avoiding immune recognition, and extending their blood circulation [51], [58], [59]. PEGylation can be done by covalent linking or by adsorbing PEG chains onto the surface of the NP. In this case, PEG methylated with a thiol end was used because of the high strength of the thiol-gold quasi covalent bond (approximately 200 kJ/mol) [58], [59].

## 1.3 Laser ablation in medicine

Light has been applied in the medical field for imaging diagnosis and surgery for quite a long time. Depending on the type of procedure, during imaging, the invasion should be minimized, while, in surgeries, lasers with more energy are mostly used for tissue ablation [60]. Laser ablation is achieved using a laser and a medium, which transports the laser light inside the cells. The laser is composed of a power source, a medium, and a reflecting mirror. These reflecting mirrors deliver a monochromatic light with a specific wavelength that defines the laser's properties and the interaction with biological tissue.

Laser-tissue interaction can be described by three main optical events: scattering, reflection, and absorption [60]. The light and tissue interaction depends on the tissues' optical property and the light source's wavelength. Since the optical property of tissues and biomolecules are difficult to modify, the selection of the wavelength of light for medical use should be the focus. The light absorbed/accumulated may have a catalytic effect on the tissue, affecting metabolic pathways (changing the enzyme activity) or causing a photothermal effect. The photothermal effect is influenced by the laser light wavelength (depending on the wavelength, the penetration level on the tissue differs as well as the energy applied), laser settings (laser power, energy, and treatment time), and physical properties of the tumour cell. In photothermal procedures for cancer therapy, heat is crucial since tumour cells are more susceptible to temperature variation. [61]–[63].

### 1.3.1 Phototherapy at the nanoscale

The most common phototherapy methods for treating cancer are photodynamic therapy (PDT) and photothermal therapy (PTT). PTT and PDT are two minimally invasive therapeutic methods, having promising potential in the diagnosis and prevention of cancer. The difference between the two is that PTT is referred to as the induction of localized therapeutic temperature, that stimulates hyperthermia physiological responses. In contrast, PDT uses a photosensitive agent that generates ROS, causing cell death by apoptosis and necrosis [64].

Conventional phototherapy still faces limitations such as limited efficiency and difficulties in heat dispersion or tissue penetration depth. Nanomaterials, more specifically noble metal NPs, have attracted attention in PTT due to their physical-chemical properties that could improve the phototherapeutic outcomes [65]. AuNPs are mostly used in PTT, due to their efficient ability to photothermal conversion, by using the SPR effect. The optical energy obtained by the oscillating electrons turns into heat and transfers via electron-phonon relaxation at the maximum amplitude of the oscillation at the specific wavelength band (SPR) of the NPs [66]–[68].

The photothermal conversion efficiency of plasmonic nanostructures is highly dependent on the absorption efficiency. The optical features of plasmonic materials are based on absorption, scattering, and extinction. The relative ratio of scattering to absorption (Csca/Cabs) increases with the nanosphere diameter. NP with a higher diameter absorbs in the NIR spectrum, as a result, most NPs used in PTT use NIR lasers since the NPs photoconversion efficiency is enhanced. NIR lasers are commonly used in PTT due to the optical window, where haemoglobin, melanin, and water absorption are reduced, allowing a deeper light penetration in the tissues [69]. However, the downfall of using AuNPs with a higher diameter in the NIR is that the scattering component is higher, implying a higher loss of energy [70]. In visible light, the AuNPs have a smaller diameter, thus exhibit higher light-to-heat conversion efficiency due to the high absorption efficiency. Regarding the use of visible light in medicine, green lasers have been used in ophthalmic laser procedures for photocoagulation as a safe tool for tissue ablation, such as in retinoblastoma and cataract surgery [71]. In this work, AuNP were irradiated with a green laser that emits with a wavelength of ~532 nm.

### 1.3.2 PTT and hyperthermia

Hyperthermia is a therapeutic concept in photothermal therapy that indicates the rise in body tissues' temperature by radiofrequency, microwave, ultrasound, perfusion methods, or light [72]. Hyperthermia is divided into the following three categories: local, regional, and whole-body hyperthermia. Local hyperthermia is applied directly to tumour sites where the tumour is superficial, unlike regional hyperthermia is applied locally in advanced or recurrent tumours. The whole-body hyperthermia is used to treat disseminated/metastatic diseases like, for example, malignant melanoma [73]–[76].

Temperature is a critical component in all thermal laser-tissue interactions. Depending on the increment of temperature and duration of exposure, different effects may occur

including apoptosis, necrosis, coagulation, and vaporization. Hyperthermia induces numerous changes in cellular physiology, as it is described in figure 1.8. Thermal ablation usually occurs when the increased temperature in tissue is above 50 °C to induce irreversible cellular damage. In contrast, hyperthermia corresponds to the increment of temperature (in a range between 37-42 ºC) that stimulates hyperthermia physiological responses [63], [76], [77]. Hyperthermia causes changes in a biomolecular level such as inhibition of DNA synthesis, increased degradation of aggregated/misfolded proteins, disruption of the membrane cytoskeleton, as well as metabolic changes that lead to a decrease of the ATP levels and alterations on the membrane permeability [74], [75], [78]. In hyperthermia, the temperature rise is based on the threshold of the irreversible thermal cell damage. The clinical efficiency is influenced by different factors as cell type, cell cycle, physical-chemical aspects, and pH level [79].

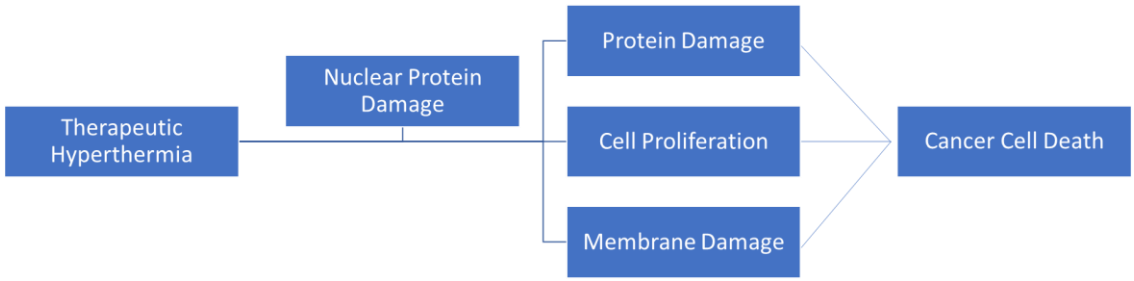


Figure 1.8: Representation of the cellular response to stress in therapeutic hyperthermia.

### 1.3.3 Hyperthermia and the effects on cancer metabolism

The biological effects of hyperthermia lead to an alteration of the extracellular microenvironment, such as activation of immunological responses, enhancement of tumour blood flow, permeability, and increased tissue oxygenation [75], [80]. A solid tumour has several critical properties compared to normal tissues, including lower values of pH and oxygen levels, abnormal vascular network (e.g., heterogeneous, and chaotic vessel growth), accumulated substantial stress because of the rapid tumour growth, and elevated interstitial fluid pressure (IFP) due to the increased permeability of the tumour-associated vasculature combined with the lack of functional lymphatic drainage. As a result, this

environment makes tumour cells more sensitive to heat than normal cells setting the rationale for the use of hyperthermia, especially as a adjuvant therapy [79], [81], [82].

Hyperthermia affects the tumour microenvironment, most likely by a temperature-sensitive regulator involved in tumour vascular perfusion and tumour metabolism. Hyperthermia boosts the immune response by activating heat shock proteins (HSPs), the primary heat response regulators present in the cell membrane [79], [83]. Hyperthermia also influences antigen presentation, inflammatory cytokine expression, and lymphocyte trafficking. Nevertheless, protein denaturation is the leading cell death mechanism caused by hyperthermia.

## 1.4 Combination treatment for cancer therapy

Cancer treatment requires the supportive efforts of multiple medical specialties. Although surgeons are often the first specialists to treat cancer patients, the array of cancer treatment alternatives is continuously expanding, requiring integrated multimodality treatment. Chemotherapy is the most widely used treatment in most types of malignancies. Chemotherapy uses one or more chemical anticancer drugs as part of a standardized regimen intending to cure, prolong life, or reduce the symptoms of cancer [84], [85]. However, in most cases, the patient presents side effects from the treatment because of the treatment's inability to deliver drugs that distinguish tumour effects from normal tissue toxicity. Besides, drugs are administrated to the patient by oral or intravenous routes, per consequence the body's metabolic system tries to slow down the administration of the drug pharmacokinetics behaviour thus lowering the therapy's efficiency.

Another problem that chemotherapy brings is how cancer cells develop resistance to chemotherapeutic agents/drugs, known as multiple drug resistance (MDR). This phenomenon is associated with tumour cells' resistance to the cytostatic or cytotoxic actions to a variety of chemically and functionally anticancer drugs. The drug resistance mechanisms have been discussed through several works and can be generalized to the following mechanisms: (a) over-expression of ATP binding cassette (ABC); (b) efflux transporters; (c) decrease in drug uptake; (d) increase in DNA repair; and (e) inactivation of chemotherapeutic drugs by metabolic enzymes [86]–[89].

Most anticancer drugs have a narrow therapeutic index, develop MDR, and present unspecific biodistribution on intravenous/oral administration, leading to severe side effects for healthy tissues. A combined therapy accomplishing three main points that were not possible with a single-agent therapy: (a) provides a more specific treatment; (b) reduces the side effects increasing the life quality of the patient; and (c) reduces the neces-

sary dose for the treatment [88], [89]. Therefore, gene therapy emerges as a possible solution, proving a better understanding of tumourigenesis's molecular and genetic mechanisms as well as allowing combinatory therapy approaches [90], [91].

### 1.4.1 Gene therapy and nanotechnology

Gene therapy has been receiving increasing attention in tumour suppression, due to the possibility of downregulating specific oncogenes' expression or sensitizing cells in an intracellular targeting process. RNA interference (RNAi) is mostly used as an effective process of sequence-specific post-transcriptional gene silencing, being an economic, fast, and efficient method for cancer therapy. The RNAi molecules are delivered into cells and initiate the degradation of the complementary mRNA molecules via cell's internal machinery, consisting of enzymes Drosha and Dicer, responsible for the cleavage and degradation of mRNA. This halts the production of the proteins encoded by the mRNAs, resulting in a reduction of gene expression [92].

Small interference RNA (siRNA) has earned attention in cancer therapies, due to their potent RNAi activity. The fundamental difference between siRNA and miRNA is that miRNA is endogenous while siRNA is artificially synthesized. As a result, the miRNA acts on the 3′-untranslated regions of the target gene, whereas siRNA can act on any part of the mRNA having a higher therapeutic effect on tumour cells [93].

For gene therapy to occur successfully, an appropriate gene delivery system is required for proper cellular uptake and efficient gene transfer. Viral vectors can mediate gene transfer with high efficiency, ensuring a long-term gene expression. However, viral vectors present several drawbacks like acute immune response, immunogenicity, limitations of the inserted DNA, and difficulties in scaling into pharmaceutical products. Non-viral approaches have emerged as a possible alternative for gene transfer, characterized by having a low immunogenicity, low toxicity, and high specificity [92]. As such, NPs offer an ideal platform for gene delivery providing: (a) protection and stability of therapeutic agents against enzymatic degradation (nucleases); (b) control over the distribution in the target; and (c) targeted and sustainment delivery of genes in the target tissue [25], [92].

Molecular nanomedicine applied to cancer therapy relies on the precise, sustainable delivery and control of therapeutic agents into cancer cells. AuNPs have been used in combinatory approaches, as multifunctional agents, more specifically in photothermal therapy due to their ability to improve cellular uptake and per consequence the efficiency in gene delivery [25]. AuNPs are described as excellent efficient and specific carriers for

gene therapy, due to their ease of functionalization, enhanced cellular uptake, and low cytotoxicity. AuNPs carriers have been used for RNAi tools, such as antisense oligonucleotides (ASO) and siRNA [25]. In antisense gene therapy, ssDNA oligonucleotides may be delivered into cells, and target specific mRNA molecules inducing inhibition of the target gene expression [94].

Baptista's group pioneer uses hairpin ssDNA structures, vectorized via AuNPs, to silence any possible RNA mediated pathway inside the cell specifically. NPs have the duality of inhibiting the encoded protein expression, plus being a nanocarrier for theranostic systems [95]. The Au-nanobeacons developed are an effective molecular nanotheranostics platform, having several advantages compared to the traditional methods. Naked/unmodified oligonucleotides have some drawbacks like extremely short half-lives due to cellular RNases activity, poor chemical stability, and high cost. In contrast, these Au-nanobeacon can easily interact with biomolecules for long extended periods due their being highly soluble, homogeneous, stable, and not prone to aggregation [95]. It was also reported, that these Au-nanobeacons show a higher silencing capability compared to oligonucleotides in an *in vivo* zebrafish model for gene silencing [96].

### 1.4.2 *c-MYC* oncogene and cancer metabolism

The oncogene selected for this work was *c-MYC*, an overall well-studied biomarker for cancer. It is estimated to contribute to at least 75% of all human cancers, including prostate, breast, colon, and cervical cancers. The proto-oncogene *c-MYC* encodes a transcription factor, regulating cell proliferation, growth, and apoptosis [97], [98]. MYC protein is a helix-loop-helix zipper transcription factor that dimerizes with its partner protein Max. The MYC-Max heterodimer can repress gene expression through complex formation with the transcription factor Miz1 [99]–[101].

MYC expression is regulated by normal stimuli, such as growth factor signalling, when cells enter the cell cycle and proliferate for tissue repair [100], [102]. *c-MYC* mRNA is short-lived, and in normal tissues, positive regulatory signals are absent, and the *c-MYC* transcription decreases, providing no abnormal proliferative growth. However, in tumour cells, the *c-MYC* function is almost always increased by mutations in the gene itself, commonly through the induction of *c-MYC* expression via upstream oncogenic pathways. [99], [101].

## 1.5 Objectives and Framework

Following our previous statements, cancer is a heterogeneous disease with diverse biological presentations, epidemiology, responses to treatment, and prognosis. As a result, cancer is one of the leading causes of morbidity and mortality worldwide. Surgery is still the first option and the most effective way to remove a tumour and promote cancer-free life expectancy. Unfortunately, this approach often fails, leading to relapse and diminishing patients' quality of life. The field of nanomedicine provides effective multifunctional nanocarriers for a range of innovative therapeutic strategies in cancer therapy, with the advantage of being less invasive and more specific. Gene therapy is a form of treatment that utilizes genes to treat an illness using a carrier and an oncogene or tumour suppressor. These therapies can include metal NPs suitable for targeted delivery of drugs (e.g., nucleic acids), coupled to novel strategies, such as photo-induced hyperthermia. This effect may be enhanced by the photothermal conversion of a light source in the visible spectral region and improve current therapeutic strategies. Noble metal NPs are mostly used in hyperthermia since the visible laser will trigger an enhanced photothermal conversion, destroying the cancer cells and reducing the tumour volume.

The present work aims to use AuNPs, a multifunctional nanocarrier, for combined cancer therapy for gene silencing and as a photothermal agent in the target colorectal tumour cells. The approach used in this work is presented in Figure 1.9.

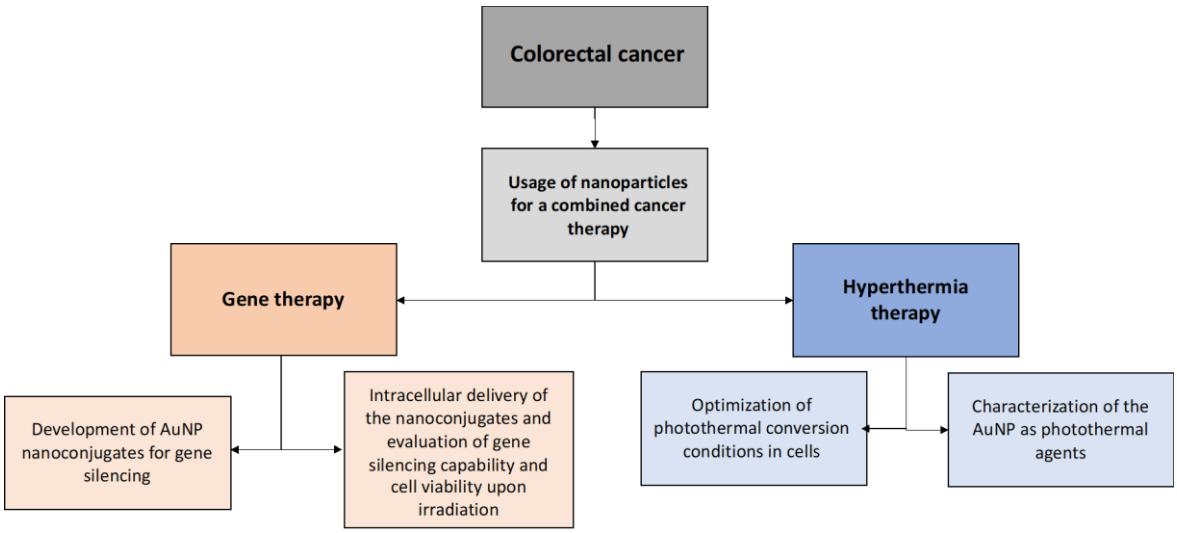


Figure 1.9: Representation of the thesis' goals and the designed approaches.

# 2 Materials and methods

In the following, it is described as the methods used for synthesized, characterized, and functionalized the AuNPs. Afterwards, the stability assays studies were performed followed by the actinometry, the cell culture, and the ICP-AES analysis. The work finalizes with the RNA extraction and cDNA synthesis for the RT-qPCR analysis.

## 2.1 Synthesis of spherical AuNP

The AuNP were synthesized following the citrate reduction method, described by Lee and Meisel [103]. The chemical synthesis of AuNPs is achieved through the reduction of gold salts to zero valence atoms, from $Au^{3+}$ to $Au^{0}$. The citrated-capped AuNP (AuNP@citrate) are negatively charged and attract positively charged cations from the solution, thus forming a diffuse electrical double layer preventing the aggregation of the NPs [51], [104]. The size of AuNPs is controlled by the ratio of concentration between the citrate and tetrachloroauric acid added to the solution [104].

Before the synthesis of AuNPs, the glass material was treated with *aqua regia* (3:1 HCl: $HNO_3$). Afterwards, the material is washed with distilled water and Milli-Q water to ensure pH 7. The solution tetrachloroauric acid (225 mL, 1 mM) was heated and put under rapid stirring to guarantee the solution's homogenous heating. When the solution was boiling, it was added a hot aqueous solution of trisodium citrate (5 mL, 2% w/v). The solution colour changed from pale yellow to transparent and then deep red, due to the formation of AuNPs. Afterwards, the solution was continuously stirred for 15 min and allowed to cool at room temperature. AuNP@citrate were sterile filtered using a 0.2 μm syringe filter and stored in the dark at 4 °C until further use.

## 2.2 Functionalization of the AuNP with PEG

Polyethylene glycol (PEG) is a coiled polymer of repeating ethylene ether units with dynamic and flexible conformations. PEG is characterized as a hydrophilic biocompatible molecule with low toxicity [105], [106]. In this work, the AuNPs were functionalized with a commercial hetero-functional polyethylene glycol-modified with a 350 molecular weight (g/mol). The functionalization was done by using the protocol of Conde et al. [54]. An AuNP solution (10 nM) was incubated with 0.028 % (w/v) SDS and PEG for a period of 16 h under agitation at room temperature. The excess of PEG chains was removed by centrifugation at 14000×g for 40 min at 4 ºC. The degree of PEG coverage on the AuNP surface was evaluated via Ellman’s Assay, to quantify the thiols free in

solutions [107]. The Ellman´s calibration curve is showed in Annex D. The AuNPs functionalized with PEG (AuNP@30%PEG and AuNP@100%PEG) were further characterized by UV-Vis, DLS, and ZP, as described in the 2.3 section.

## 2.3 Characterization of the AuNP

### 2.3.1 Characterization of the AuNP by UV-Vis

The characterization of the AuNP was performed through an empirical UV-Vis spectroscopy method, discussed by Haiss et al. [108], where it was possible to estimate the diameter of spherical AuNP using the SPR and the molar extinction coefficient [109]. The concentration of the AuNPs was calculated by applying the Lambert-Beer equation.

The equipment used was a spectrophotometer UV-3101 PC UV/visible/NIR double beam spectrophotometry (Shimadzu, Kyoto, Japan). Triplicated UV-Vis spectra measurements were taken in the 800-400 nm wavelength range with 1 cm path quartz cuvette at room temperature, from 1:10 dilutions of the AuNP@citrate colloidal suspension. For the AuNP functionalize with PEG (AuNP@PEG), UV-Vis spectra were taken from 1:100 dilutions since these NPs were highly concentrated.

### 2.3.2 Characterization of the AuNP by DLS and ZP

DLS and ZP analysis was determined by resorting to a Nanoparticle Analyzer SZ-100 at 25 ºC for the analysis of the NPs hydrodynamic diameter and surface charge [110]. The AuNP formulations were diluted in Milli-Q water to a final concentration of 1 nM, to avoid the filter's saturation. The analysis was performed at 25 ºC, with a scattering angle of 90º, using Milli-Q water as a medium of dispersion, having a total of three measurements performed for each sample.

## 2.4 AuNP stability assays

The AuNP were subjected to increasing ionic strength solutions to assess different media's effect in the prepared AuNP conjugates, to further analyse their aggregation profile. If the PEG's functionalization was adequate, the conjugates would sustain higher ionic strengths without aggregating [111], [112].

These stability assays were performed by Rafael Paiva as part of his undergraduate project (LBCM) and included here with his approval. The stability assays were tested in different types of solution: NaCl with different concentrations for testing the ionic force

(from a range of 0-5 M) and PBS along the time (0-120 min) to simulate the osmolarity and ion concentrations of the human body (isotonic).

## 2.5 Actinometry

The actinometry measurements were performed with Aberchrome 540TM, E-form ((E)-a-(2,5dimethyl-3-furylethylidene)(isopropylidene), a chemical actinometer used to quantify the number of photons in a beam integrally or per unit time. The Aberchrome 540, E-form ((E)-a-(2,5-dimethyl-3 furylethylidene)(isopropylidene) succinic anhydride) when irradiated with UV light at a wavelength of 350 nm, converts the original colourless solution to red, indicating the conversion to the C-form (7,7a- dihydro-2,4,7,7,7a-pentamethylbenzo [b] furan-5,6-dicarboxylic anhydride) [113], [114].

For these measurements, a solution of 200 µM of Aberchrome 540 was dissolved in 2 ml of absolute ethanol. Afterwards, the Aberchrome 540 was irradiated with a UV lamp with a 366 nm filter until a photo-stationary state, related to C-form's maximum conversion, was achieved. The C-form solution was irradiated with the green laser with a wavelength of 532 nm diode-pumped solid-state laser coupled to an optical fibber (DPSS) (Changchun New Industries Optoelectronics Tech. Co., LTD, Changchun, China). The solution was analysed by UV-Vis spectroscopy, where three measurements were taken in the 300-550 nm wavelength range with a 1 cm path quartz cuvette at room temperature. It is important to notice that the Aberchrome 540 solution should be prepared fresh as it must be protected from the light, to avoid any interferences in the chemical actinometer spectra.

## 2.6 Cell culture

The HCT116 cells are epithelial adherent tumour cells, characteristic of CRC in humans. These cells are colon epithelial cells, responsible for the constitution of tissue from the colon mucosa, commonly used in preclinical model systems for studying tumourigenesis [115], [116]. This cell line was selected since it is one of the most studied cell lines in the present laboratory, being the most versatile and simple to maintain in the laboratory.

HCT116 colorectal carcinoma (ATCC® CCL-247™) were grown in DMEM with phenol red (pH indicator with red coloration) and supplemented with 10 % (v/v) FBS and 1 % (v/v) antibiotic/antimycotic. The cell lines were cultivated in T-flasks with 75 $cm^2$ (SPL Life Sciences, South Korea). The cells were kept in a $CO_2$ incubator (SANYO $CO_2$

Electric Biomedical Co.) at 37 ºC, 5 % (v/v) $CO_2$, and 99 % (v/v) relative humidity. Analysis of mycoplasma was performed weekly through PCR, tested by a lab technician.

## 2.7 Cell viability assays

The cell viability was analysed via two different methods, colorimetric with MTS and, staining with Trypan blue. MTS assay is a sensible colorimetric method that quantifies the formazan produced, which consequently is directly proportional to the number of viable cells. Trypan blue assay is a rapid and straightforward technique that consists of the principle that intact cell membranes exclude certain dyes, while in compromised membranes the dye penetrates making it possible to access the cell permeability [117], [118].

During irradiation experiments, DMEM without phenol red was used to avoid any interference in the samples irradiated. The DMEM medium with phenol red is a solution with red coloration, as such it absorbs the visible light of the green laser, heating the solution. The cell viability assays were performed throughout the work in a 96-well plate. The 96-well plate was used to guarantee the same reproducibility but mostly due to the laser irradiation, since the surface area of a 96-well plate is the same diameter as the light emitted by the green laser.

The Trypan blue assay was performed right after the microplate's irradiation, to evaluate the cell membrane's damage. It was added 100 µL of Trypan blue to cover the microplate well completely, and after 5 min, it was washed with PBS to remove the excess. MTS assay was performed 18 h after irradiation, based on studies previously done for photothermal assays [113]. After removing the medium, the MTS solution was added in the right ratio (80:20) and incubated for 45 min. The absorbance of the samples was analysed at 490 nm. The cell viability was determined by subtracting a blank to all experiments and dividing its absorption by control, as is shown in Equation 1. Concerning the calculation of the cell viability, three independent biological assays were performed.

$$Cell\ Viability\ (\%) = \frac{mean\ Abs.of\ treatment\ group}{mean\ Abs.of\ control\ group} \times 100 \qquad (1)$$

Statistical significance of all data was verified by One-way ANOVA test, performed with GraphPad Prism 6.0 (GraphPad Software, Inc). The Tukey method allowed to determine statistically significant differences between the samples and results were considered statistically significant for $p < 0.05$ (Annex E).

## 2.8 ICP-AES (Inductively Coupled Plasma – Atomic Emission Spectroscopy)

ICP-AES is an analytical technique used for the detection of chemical elements. ICP-AES is an emission spectroscopy method that excites atoms and ions with a plasma, causing it to emit electromagnetic radiation at characteristic wavelengths. The quantification is based on the Lambert-Beer equation, where the intensity of characteristics wavelengths is proportional to the ions/atoms' concentration.

The ICP-AES was performed at REQUIMTE, a laboratory that helps in technical resources of chemical analysis in FCT-NOVA. For ICP-AES analysis, the cells were seeded in a 96-well plate with a cell density of $2\times10^4$ cells per well. There were two types of samples analysed, the supernatant and the cells with AuNP (with/without irradiation). *Aqua regia* is prepared previously and then added to the falcon tubes. The ICP-AES analysis requires a control sample with the same material density (5 mL) as a blank, to avoid any measurements' interference. The supernatant (1 mL) was stored in 15 mL falcon tubes, and PBS was added to wash the cells. Trypsin was added to detach the cells, centrifuge at 300 ×g for 5 min and then added *aqua regia*, before being stored at 4 ºC.

## 2.9 Cell challenge and gene expression

The cells were seeded in a 96 well-plate with a density of $2\times10^4$ cells/well. For the hyperthermia characterization, the AuNP were challenged for 4 h. This time point was based on previous work done in the laboratory, proven by Pedrosa, where the AuNPs have an optimal uptake by the cells between 4-7 h. After this period, the AuNP reaches a plateau in the cellular uptake as the NPs tend to aggregate [113].

For the gene expression, the cells with a density of $2\times10^4$ cells/well were challenged with the AuNP@PEG@MYC, provided by David Fontinha, with a time point selected of 6 h. The challenge was performed with 0.6 nM of AuNP@PEG@MYC corresponding of 36 nM of oligonucleotides (ratio of Au:oligonucleotides = 1:60). The control used was cells with AuNP@PEG at 0.6 nM. The cells were later centrifuged at 200 ×g for 5 min at room temperature, and the total RNA was extracted from the cellular pellet.

### 2.9.1 RNA extraction and quantification

The RNA extraction protocol was adapted for a 96-well plate; 100 µL of Trisure was added to 5 well from the 96-well plate to ensure the sufficient extraction of RNA (total volume of 500 µL). Afterwards, the samples were incubated with the Trisure for 5 min at room temperature and 0.2 mL of chloroform was added. Then the solution was

transferred into centrifuge tubes of 1.5 mL and then centrifuge for 12000 ×g for 15 min. It is essential to shake the tubes vigorously so that the aqueous phase be on the top, to facilitate the RNA extraction.

After transferring the aqueous phase carefully, the RNA was precipitated by adding 0.25 mL of isopropyl alcohol. The RNA precipitation efficiency was enhanced by storing the solution at -20 ºC overnight and by adding 1 µL a solution of acetate sodium 3 M, pH 5.5. Afterwards, the tubes were centrifuged at 12000 ×g for 10 min, the supernatant was removed, and centrifuged at 7500 ×g for 5 min after adding ethanol to clean the samples. Lastly, the samples were left dry at room temperature to remove any remaining ethanol and re-dissolve the RNA in PCR water incubating for 10 min at 60 ºC.

The RNA samples were transported on ice to the spectrophotometer, then it was loaded 2 µL of Milli-Q water as the blank and then 2 µL of the sample was loaded to quantify the RNA extracted. It is important to register the A260/A280 and A260/A230 absorbance ratios, to evaluate the quality of the RNA.

### 2.9.2 cDNA synthesis

Reverse transcriptase (RT) is an enzyme that uses an RNA template to generate complementary DNA (cDNA). As such, it is possible study mRNA expression via methods such as RT-PCR (Real-Time polymerase chain reaction) [119].

The total RNA extracted from samples was reverse transcribed using the NZY M-MuLV First-Strand cDNA Synthesis kit. The conversion of the RNA to cDNA is done on ice and in a sterile nuclease-free microcentrifuge tube, where initially a master mix without RNA is prepared. The final volume for the reaction used was 10 µL. The components were mixed gently and incubated at 25 ºC for 10 min, then 37 ºC for 50 min, and heating at 85 ºC for 5 min. The samples were then chilled on ice and added 1 µL of NYZ RNase H and incubate at 37 ºC for 20 min (this step is for RNA removal, to enhance the sensitivity of the PCR).

### 2.9.3 Real-time polymerase chain reaction (RT-qPCR)

RT-qPCR is a powerful tool to quantity gene expression by measuring the amount of cellular RNA, and so, is a rapid, sensitive method for analysing gene expression. The quantitative endpoint for a real-time PCR is the threshold cycle (Ct) as the fluorescent signal, where the numerical value of the Ct is inversely related to the amount of amplicon in the reaction [120], [121].

The controls in PCR are crucial since positive controls can provide consistent positive reference data points in each experiment and negative controls for external contamination or other factors, resulting in a non-specific increase in the fluorescence signal. The most used method to control sample-to-sample variation, due to biological effects, is based on a reference gene. The reference gene is assumed to have equal expression levels in each experimental sample; in this case, the reference gene was 18S [121].

Relative or comparative quantification uses Ct's difference to determine the differences in the target sequence's concentration in different samples. The qPCR data were analysed by the Ct method (2-ΔΔCt) [121]. The relative gene expression level is calculated by quantifying the gene of interest (*c-MYC*) compared to the control gene (18S), normalized to the control condition (cells exposed to AuNP@PEG):

$$\Delta Ct = Ct_{c-MYC} - Ct_{18S} \qquad (2)$$

$$\Delta\Delta Ct = \Delta Ct_{treated} - \Delta Ct_{untreated} \qquad (3)$$

RT-qPCR was performed with a time point of 6 h of incubation. This time point was defined, with David Fontinha's help, as the optimal time point for silencing *c-MYC*. cDNA amplification by qPCR was performed in Corbett Rotor-Gene 6000 thermocycler using NYZqPCR Green Master Mix (2×). The reaction mixture was prepared for a final volume of 20 µL with 1 µL of cDNA template and the following primers, at a concentration of 200 nM each: *c-MYC* forward (5' – GCTCATTTCTCT GAGGACTTGT - 3') and *c-MYC* reverse (5' - AGGCAGTTTATATATATGGCTAAATC – 3'); 18S forward (5'-GTAACCCGTTGAACCCCATT - 3') and 18S reverse (5' - CCATCCAATCGGTAGTAGCG - 3'). QPCR conditions included an initial denaturation time at 95 ºC for 5 min and 40 cycles of 95 ºC for 20 s, 55 ºC for 20 s, and 72 ºC for 30 s.

Statistical significance of all data was verified by One-way ANOVA test, performed with GraphPad Prism 6.0 (GraphPad Software, Inc). The Tukey method allowed to determine statistically significant differences between the samples and results were considered statistically significant for $p < 0.05$ (Annex E).

# 3 Results and discussion

### 3.1.1 Characterization of the AuNP by UV-Vis

UV-Vis spectroscopy is a useful technique, providing information about the size and concentration of AuNPs. Size estimation of colloidal AuNP may be attained via the spectral data's interpolation, as described in figure 3.1 [109]. This analysis considers the absorbance at 520 nm (SPR) and 450 nm, whose ratio is proportional to the core size. Of course, under this approach, there are some simplifications and some limitations. First, it is well suited for analysing small spherical AuNPs with a normal distribution of diameters in a steady and stable media [109]. Any changes to the medium dielectric and surface of the AuNPs, induce dramatic changes that introduce a considerable bias to the use of this approach. Still, due to its simplicity and seemingly straight forward, the above-mentioned spectral approach was used.

Figure 3.2 shows the UV-Vis spectra taken for all the synthesized and functionalized NP and nanoconjugates (AuNP@citrate; AuNP@30%PEG and AuNP@100%PEG). The concentration of the AuNP was calculated via the Lambert-Beer equation using an molar extinction coefficient of $2.33\times10^{8}$ $M^{-1}$ $cm^{-1}$ [109]. As a result, the working solutions showed a concentration of 10.13 nM, 95.99 nM, and 93.84 nM, respectively. The AuNP@PEG has a higher concentration due to the functionalization process which implies high-speed centrifugation.

A closer observation of the SPR peak position shows a right shift when comparing the AuNP@citrate with the functionalized AuNP@PEG. This shift is better analysed when doing the moving average of the absorbance of each condition tested, as it showed in figure 3.3. The right shift appears due to PEG covering the AuNP surface, changing the NPs plasmon behaviour. Indirectly, the shift may also indicate a slight variation of the size of the AuNP-conjugate since the surface is cover with PEG. However, it is essential to point out that the increase in size is not very accurate since PEG is a flexible polymer, having different conformations on the surface of the AuNP [122].

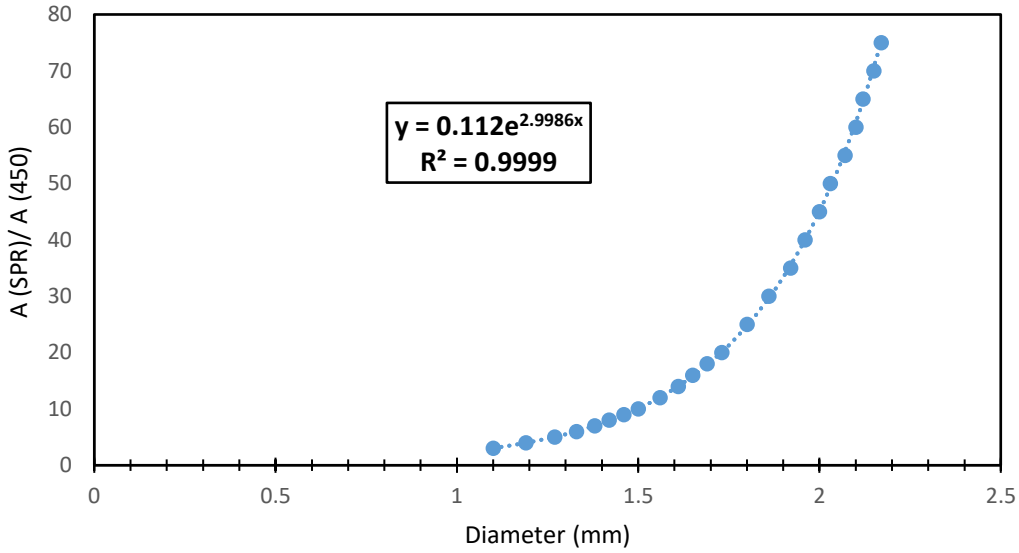


Figure 3.1: Calibration curve using the method developed by Haiss et al. [108], it was possible to calculate an approximation of the size in diameter of the metallic core of the NPs. The procedure was done by taking the absorbance values of 450 nm and 520 nm, calculate the quotient and then substitute the value (y) in the function equation shown inside the figure.

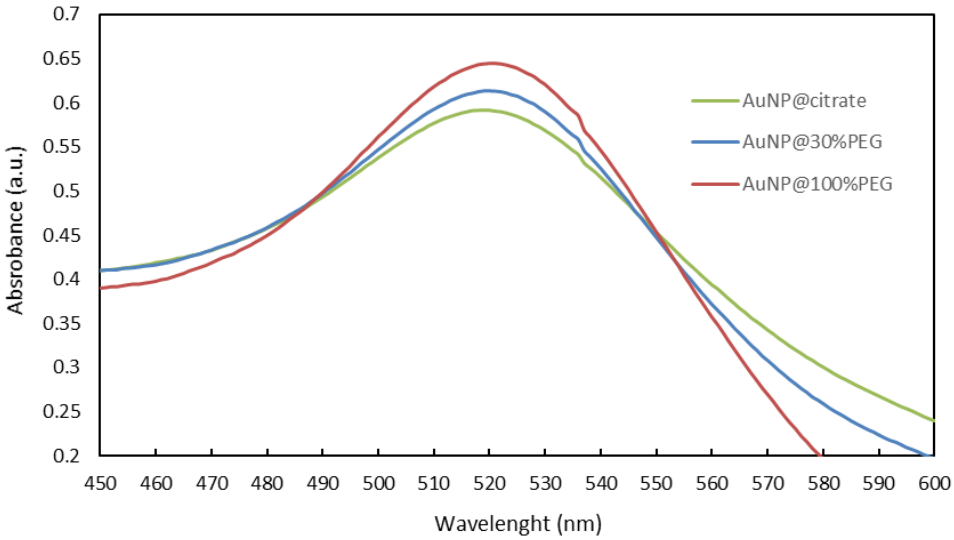


Figure 3.2: Visualization of the SPR band of each AuNP characterized by UV-Vis. SPR peaks are at 519, 520, and 522 nm, corresponding respectively to AuNP@citrate, AuNP@30%PEG, and AuNP@100%PEG. It is possible to infer a slight variation in the SPR band due to the presence of PEG.

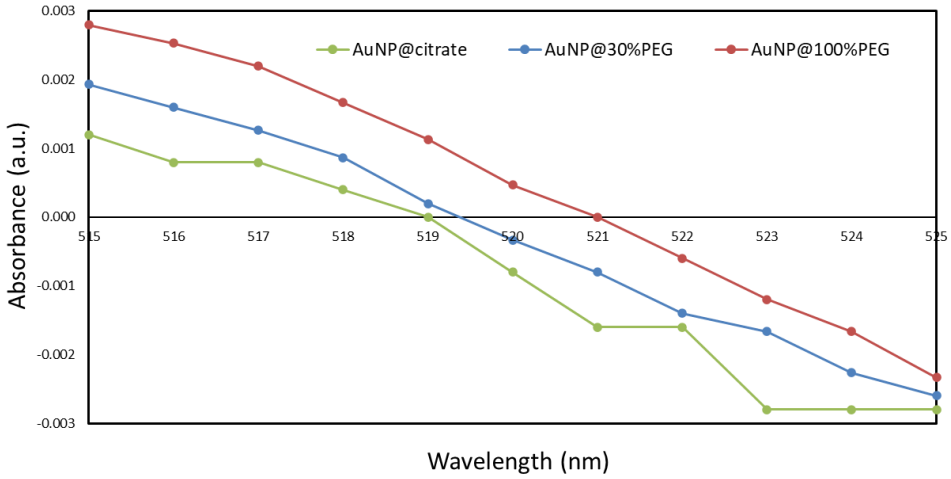


Figure 3.3: Representation of the moving average of the absorbance values corresponded to the SPR band in the UV-Vis spectra for each condition tested. The results were treated to better visualize the SPR shift between the nanoconjugates, where it is possible to observe a higher shift as the % of PEG is increased in the AuNP.

For hyperthermia, AuNPs exhibit excellent properties as photothermal agents, such as their versatility, high specificity for the target tissue and strong efficiency on photo-conversion by taking advantage of the SPR effect [66], [123]. In terms of the UV-Vis spectrum of the AuNPs, it is important to characterize the SPR band of the NPs to verify if there is any aggregation present on the solution or alteration of the SPR band. In this case the PEG is going to alter the SPR, due to the variation in size of the NPs.

### 3.1.2 Characterization of the AuNP by DLS

Dynamic light scattering (DLS) is a technique used for the characterization of the AuNP, relevant for particle size measurements. DLS is a technique used for AuNPs characterization to measure the variation of scattered light of AuNPs according to their Brownian motion, thus obtaining an approximate measure of their hydrodynamic size [124]. Factors like temperature, ionic strength, and samples' concentration disturb the dielectric properties of the NPs changing their size [125]. DLS provides information about the z-average and polydispersity index, necessary for the characterization of the AuNP. The z-average is the cumulant's mean of the hydrodynamic diameter of the AuNP and the polydispersity index is calculated from the cumulants analysis of the DLS measured intensity autocorrelation function [125].

The DLS results showed a z-average for the working solutions of 16.6 nm, 17.7 nm, and 18.9 nm for AuNP@citrate, AuNP@30%PEG, and AuNP@100%PEG, respectively.

There is a noticeable increase of Z-average on the AuNP@PEG due to the functionalization of the NPs with PEG. As stated before, PEG is a hydrophilic molecule, so it is expected that the hydrodynamic diameter of the AuNP to increased depending on the percentage of the AuNPs' surface covered by PEG [51]. Additionally, by comparing the DLS and UV-Vis results, it is possible to infer that not only the increase in the hydrodynamic diameter of the AuNP@PEG supports the functionalization of the NPs, but also explains the right shift showed in the UV-Vis spectra in figure 3.2.

Polydispersity index (PI) measures the heterogeneity of a sample. Polydispersity can occur due to variations in size distribution or aggregation of the sample, during isolation or analysis. For biomedical applications it is crucial to obtain a homogenous and monodisperse solution. As such, the ideal PI for polymer-based NPs materials is below 0.2 [126]. Figure 3.4 shows the particle frequency band, indicating the size distribution of each AuNP. Comparing the AuNP@PEG, The AuNP@100%PEG shows a PI of 0.15 as for the AuNP@30%PEG, a PI of 0.29.

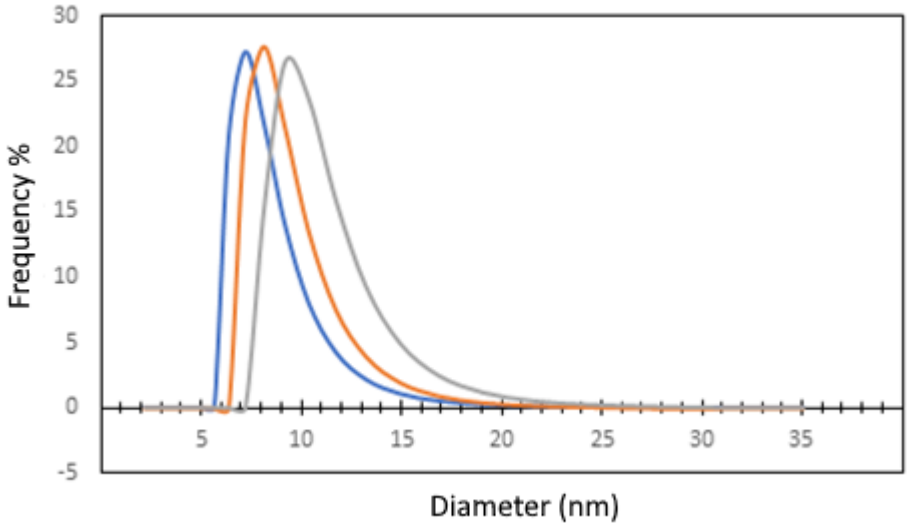


Figure 3.4: DLS measurements show the different AuNP, where it is presented from left to right AuNP@citrate, AuNP@30%PEG, and AuNP@100%PEG, respectively. From the DLS results, it is possible to observe a distinctive difference due to the variation in the size of the NPs.

The functionalization of the NPs is critical to take into account, more specifically, in cases where there is a combinatory therapy approach where the NP surface will be covered with other ligands like nucleic acids, proteins, and therapeutic agents [127]. Overall, the AuNP presents a low polydispersity with a z-average expected from NPs that were functionalized due to PEG increasing hydrodynamic diameter of the NPs. The AuNP@PEG has an SPR that is more proximal to the green laser wavelength (532 nm)

therefore when irradiated, their capability to convert light to heat increases enhancing their photothermal effect on the cells.

### 3.1.3 Characterization of the AuNP by ZP

The ZP is used to measure the surface charge, delivering information about colloidal stability [110]. The methoxy PEG surface has a slightly negative to neutral surface charge, depending on the pH, which is advantageous for *in vivo* applications [128]. In this case, the AuNP functionalized with different % of PEG will have a variation in the surface charge. Consequently, the ZP of the AuNP changes depending on the percentage of PEG [110].

According to what was mentioned previously, ZP data shows that the surface charge of the AuNP decreases depending on the % PEG added (figure 3.5). The results of the ZP were -39.8 mV, -45 mV, and -64.5 mV for AuNP@citrate, AuNP@30%PEG, and AuNP@100%PEG, correspondingly. AuNP@100%PEG has the most negative surface since the NPs are fully covered with PEG. AuNP@30%PEG shows the most heterogenicity, probably due to the instability of these NPs. By comparing the ZP results and DLS data, it is possible to assume that there was a successful functionalization of the NPs.

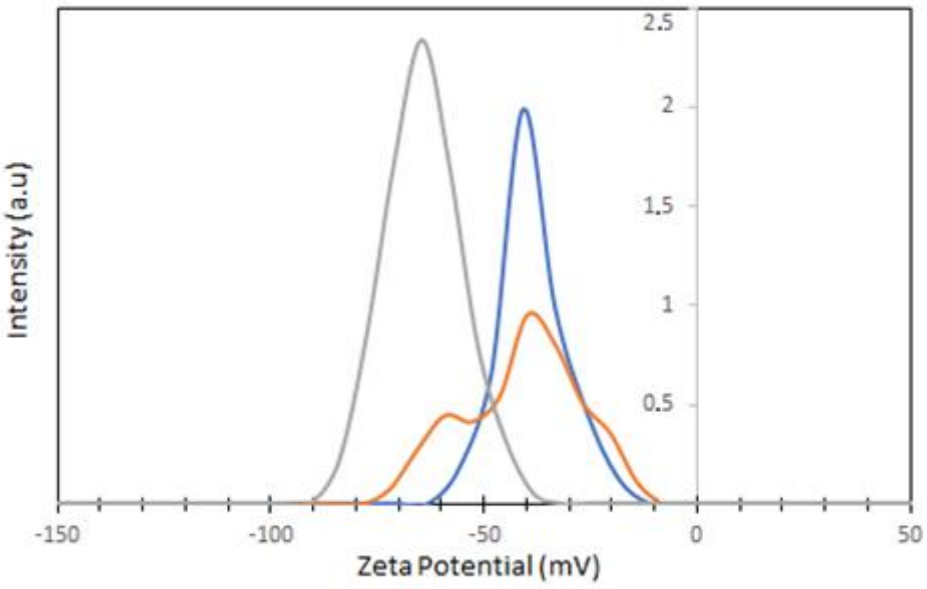


Figure 3.5: ZP measurements of the intensity concerning the charge on the surface of each NP. The ZP results show from left to right AuNP@100%PEG, AuNP@30%PEG, and AuNP@citrate, respectively.

The surface charge is essential to evaluate the AuNPs stability since it may affect the cellular uptake and the *in vivo* fate of the NPs. Cell membranes are negatively charged, and cationic agents are more easily internalized by the cells due to the electrostatic interaction. However, these cationic agents present more toxicity compared to negatively charged agents. As a result, the AuNPs are mostly internalized by endocytosis pathways with the possible activation of membrane receptors on the cell surface trigger receptor-mediated endocytosis, which is known to be a major uptake pathway for AuNPs [58], [129].

In regards of the characterization, it was possible to presume that the AuNP were successfully functionalized with the PEG thiolated supported by the characterization techniques UV-Vis, DLS and ZP. The UV-Vis results show the variation of the size of the NPs, a fact that is better observed in the DLS where it is possible to observe an increase in the NPs size as the % of PEG is increased. Lastly, the ZP shows the surface charge variation, where in result of the PEG functionalization the surface charge of the NPs is more negative compared to the AuNP@citrate. However, it is important to evaluate the AuNP@30%PEG stability under different aqueous mediums and laser irradiation, since these NPs are going to be used as a multifunctional agent for photothermal conversion and vectors for gene silencing of *c-MYC*.

## 3.2 Stability of AuNPs in different media

The stability of AuNPs is an essential requirement for therapeutic applications, more specifically, for a better understanding of the NPs behaviour *in vivo*. AuNPs are prone to aggregation if they are not coated with a capping agent that induces electrostatic stabilization. In biological systems, NPs must resist the ionic strength from the aqueous medium, preventing aggregation and loss of their physical-chemical properties, especially SPR. SPR is an optical property of noble metal NPs, that is highly influenced by the size, shape, solvent, surface ligands and charge, temperature, pH, and ionic force of the aqueous medium. Therefore, it is essential to guarantee that the SPR maintains unalterable so that the NPs can perform the photoconversion when irradiated with the green laser [36], [112].

The stability of the AuNP was studied with PBS and different NaCl concentrations (0-5 M) to simulate the osmolarity and ion concentration of the biological system. The AuNP@citrate presents a variation in the SPR band after the 0.25 M of NaCl added to the solution (figure 3.6). The AuNP@citrate does not have any capping agent that induces electrostatic stabilization to the NPs. Therefore, they eventually lose their optical properties with evident signs of NPs aggregations (observed by the solution changing from red to blue).

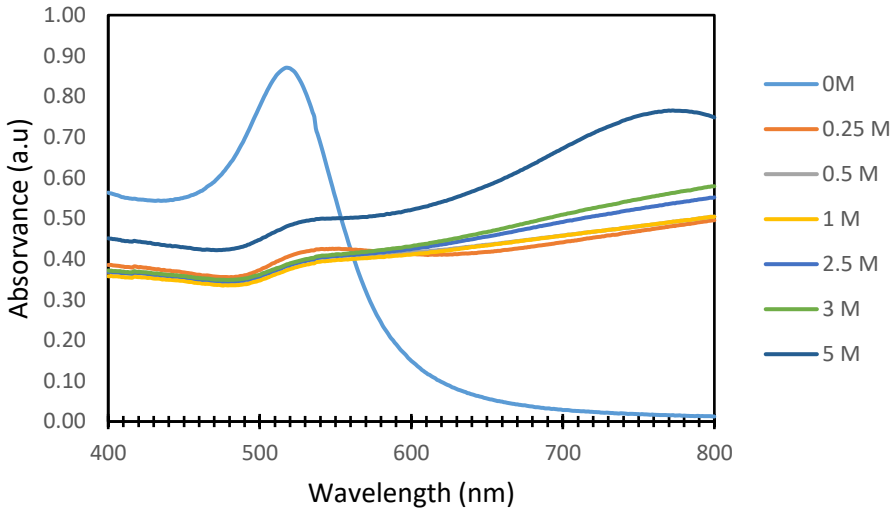


Figure 3.6: UV-Vis spectrum with the AuNP@citrate in solution with different [NaCl] ranging from 0-5 M. In this spectrum is possible to visualize the aggregation profile of the AuNP@citrate, where right after 0.25 M there are signs of aggregations with a clear shift or a complete disappearance of the SPR bands.

For the AuNP@30%PEG, the SPR is shifted to the right, as showed in figure 3.7. In this case, the AuNP is not entirely covered by PEG. The NPs resist the ionic strength but are prone to aggregation since the SPR is at a higher wavelength (~ 650 nm).

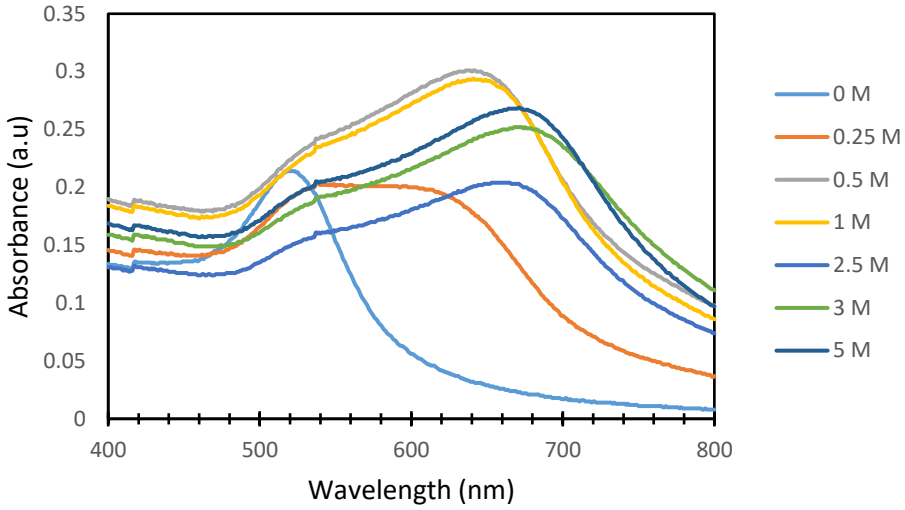


Figure 3.7: UV-Vis spectrum with the AuNP@30%PEG solution with different [NaCl] ranging from 0-5 M. The AuNP@30%PEG present a different aggregation profile, where the SPR bands shifted to a higher wavelength indicating the increase of the size of the NPs.

The AuNP@100%PEG resisted the NaCl concentration, as showed in figure 3.8, with an inalterable SPR band until 5 M of NaCl. At 5 M, the AuNP SPR suffered some alterations with a visible shift to the right. These results show that PEG is an excellent capping agent, resisting strong ionic forces as well as indicate that the NPs were successfully functionalized with PEG.

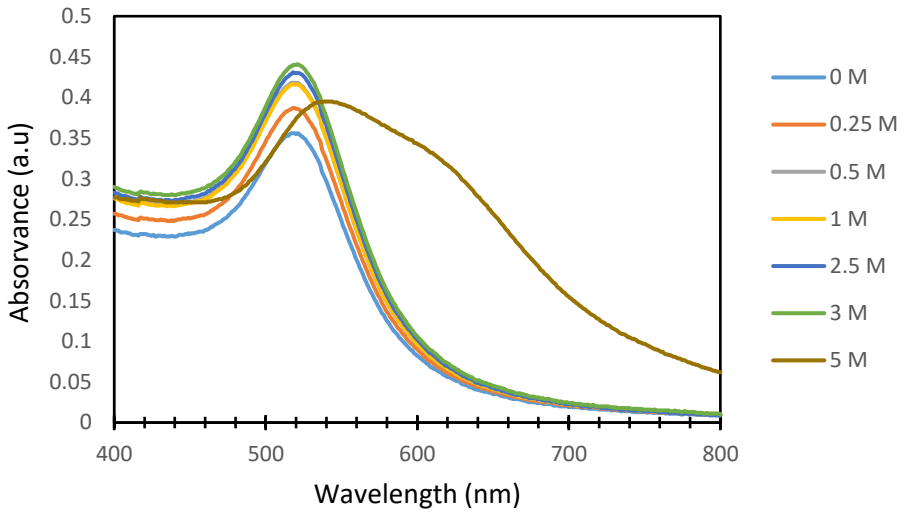


Figure 3.8: UV-Vis spectrum with the AuNP@100%PEG in solution with different [NaCl] ranging from 0-5 M. The AuNP@100%PEG present a shift at only 5 M [NaCl], presenting the highest resistance to the osmolarity and variation of ionic forces.

The AuNP@citrate, in PBS, did not resist the osmolarity, as shown in figure 3.9. AuNP@citrate presents particle aggregation signs with a drastic disappearance of the SPR band after 60 min in contact with PBS. At 120 min, it is possible to observe a straight line in the UV-Vis spectrum, indicating an almost complete aggregation of all nanoparticles with a drastic change in the NP's physical and chemical properties.

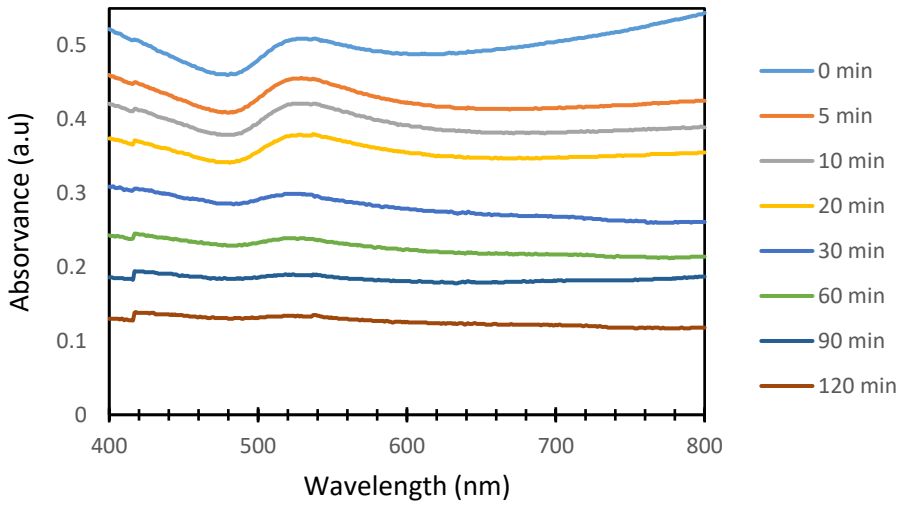


Figure 3.9: UV-Vis spectrum with the AuNP@citrate in PBS solution along the time (0-120 min). The NPs present an aggregation profile with almost the disappearance of the SPR band.

AuNP@30% PEG at 5 min has a slight shift to the right, indicating a variation in the NP's size, shown in figure 3.10. The AuNP has an increase in size since the band is around 650 nm, and the ratio of the A520/A750 is decreasing as the contact time with PBS increases (Annex C – table 5.3).

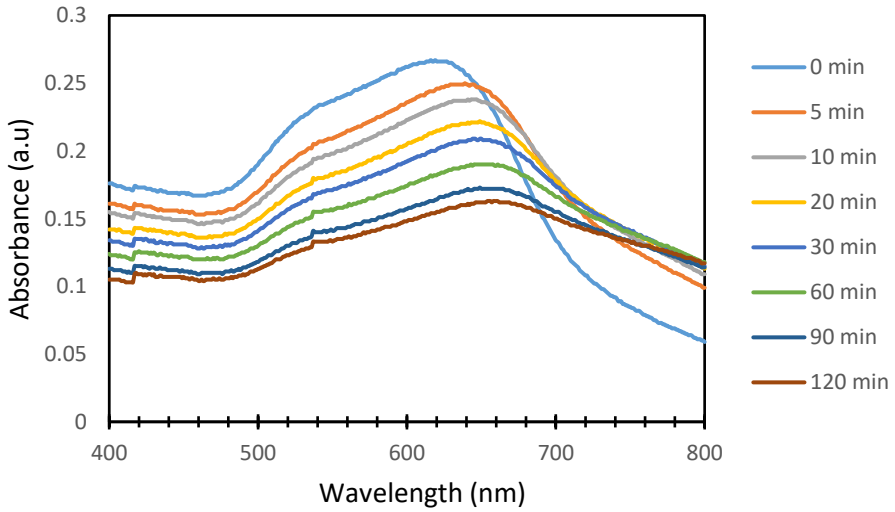


Figure 3.10: UV-Vis spectrum with the AuNP@30%PEG in PBS solution along the time (0-120 min). The NPs have the SPR band shifted to higher wavelengths in the first contact with PBS and gradually the size of the NPs increases.

The AuNP@100%PEG have more stability, as their SPR band is intact at 520 nm, during the entire time the NPs were in contact with the PBS (figure 3.11). With these results, it is plausible to assume that the AuNP@100%PEG is the most stable due to PEG's successful functionalization.

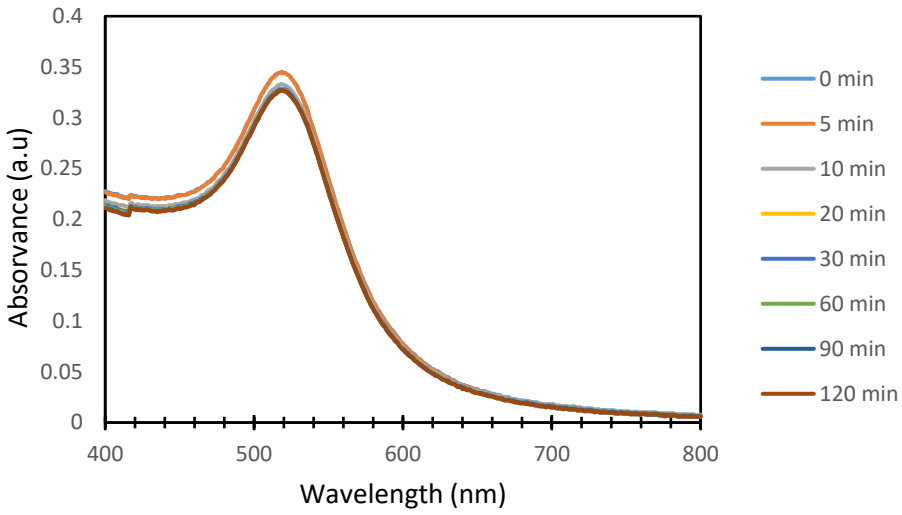


Figure 3.11: UV-Vis spectrum with the AuNP@100%PEG in PBS solution along the time (0-120 min). The NPs resistance is shown, where the SPR band maintains inalterable along with the assay.

From the stability assays, it is possible to characterize the different types of AuNP and the importance of the capping agent. Sodium citrate acts as the reducing and capping agent, stabilizing the AuNP surface during the growth phase of their synthesis [130]. According to the stability assays performed, it was possible to assume that the AuNP@100%PEG sustained and resisted when submitted to the different NaCl concentrations and in contact with the PBS. PEG is a capping agent that induces electrostatic stabilization, conferring more hydrophilicity for the NPs. As such, AuNP@PEG were further characterized as photothermal agents in hyperthermia regimens to further understand the efficiency of photothermal conversion of the NPs.

## 3.3 Actinometry

Hyperthermia is a photothermal therapy that uses heat (locally or globally) to treat cancer cells. It is essential to characterize the power source laser, to ensure that the cells receive the appropriate heat within the hyperthermia range. As such, laser characterization is an important step to evaluate the amount of energy that is being irradiated to the 96 well-plate [131], [132].

The actinometer (AberChrome 540) will measure the laser irradiation photons in the visible range (532 nm), changing the spectra due to the chemical photoconversion. As a result, it is possible to characterize the laser irradiation, with a linear relation between laser power per area and the laser current for posterior AuNP photothermal characterization [133].

Figure 3.12 demonstrates the conversion of the AberChrome 540, where it is possible to view the C form increase at 500 nm and decrease the E form at 300 nm. The maximum conversion was obtained after 110 seg of irradiation with a UV lamp with a filter of 366 nm, implying that the photo-stationary phase was achieved. Subsequently, the AberChrome 540 at the C-form will absorb the laser irradiation. It is possible to determine the number of photons in the laser power source per unit time by reconverting to the E-form. This method is proven to be very simple, rapid, and specific compared to physical approaches to study the number of photos of the laser-irradiated per area [113], [133].

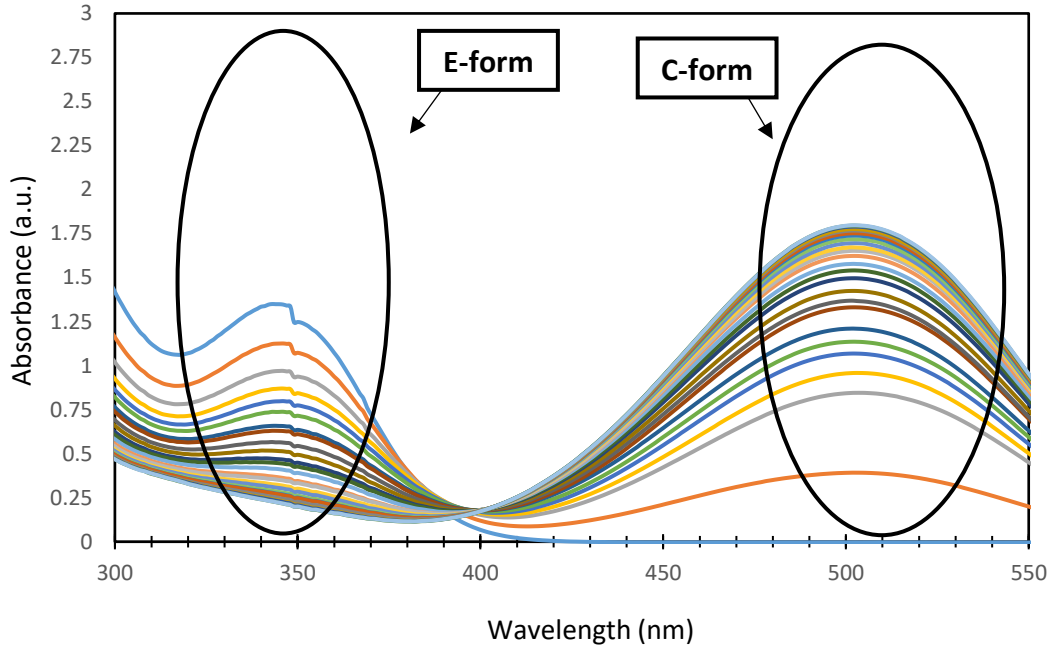


Figure 3.12: UV-Vis spectra of the AberChrome540 photoconversion. The UV-Vis spectrum was taken from 5 to 5 s in a total of 120 s. The photo-stationary phase was obtained at 110 s.

The actinometry characterization was performed by establishing a linear correlation between the laser current (mA) and the amount of energy per area received to the 96 well-plate ($W/cm^2$). It was previously defined by Pedrosa a photochemical quantum yield of 0.06 for AberChrome540, as the slope of the curve of converted moles of actinometer per absorbed photon of light, for the back reaction of C-form to E-form in ethanol [113]. With this is possible to calculate the photon flux, defined as the number of photons per second per unit area. The laser power per area is calculated by multiplying the photon flux by the energy of a single photon and dividing by the surface area of the 96 well-plate.

Figure 3.13 shows the actinometry with a linear function and the regression coefficient ($R^2$). Actinometry has the limitation of being very sensible, making it only possible

to infer the laser power per area within specific laser potencies. However, with a high $R^2$ and a linear function between the variables, it is possible to extrapolate to higher powers that will be further used in hyperthermia.

The PTT, in this work, was performed with a green laser in a continuous wave. This type of laser emits a continuous laser beam with a controlled heat output, such as laser intensity. As a result, it was possible to perform the actinometry and establish a linear correlation to evaluate the amount of laser power per area of the green laser.

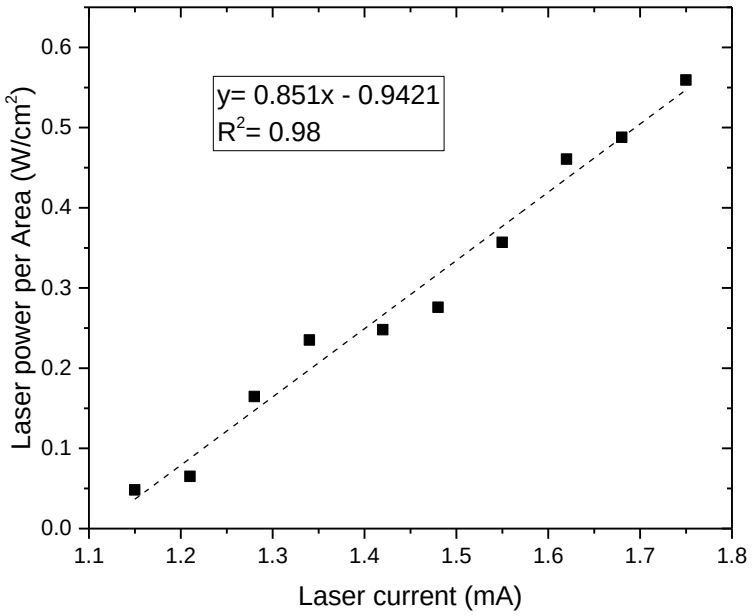


Figure 3.13: Laser calibration measurements with the linear relation between the laser power per area and the laser current. The laser current used was between 1-2 mA, where it was possible to achieve a linear function.

## 3.4 PTT system characterization

The PTT system comprises different variables, such as time irradiation, laser current, AuNP concentration, and the variation of temperature (ºC). To better understand this system's evolution and analyse more precisely the increment of temperature on the HCT116 cells, a 3D graph was constructed. Figure 3.14 shows the general evolution of the system. The parameter that has the most relevance in the variation of temperature is the concentration of NPs, as well as the laser power.

For clinical applications, it is essential to consider the cellular viability and the NP's potential cytotoxicity. Following this line of reasoning, the concentration of NPs and the

time irradiation and laser potency should be the lowest to achieve the desired efficiency. A hyperthermia regimen is achieved in the cells when the increment of temperature achieved is around 4-5 ºC. As such, the selection (indicated in the graph) was based on figure 3.15, where the time irradiation was chosen was 90 s, with a laser power density corresponding to 1.71 W/cm$^2$ with a concentration of NPs of 10 nM.

AuNP@100%PEG and AuNP@30%PEG after irradiated at 1.71 W/cm$^2$ for the 90 s were proven to be stable, however, for laser power higher (>1.71 W/cm$^2$), the AuNP begin to aggregate indicated by the solution of the well changed from red to a dark blue. With these results, it was possible to optimize the hyperthermia for these specific conditions, using AuNP@30%PEG for PTT and gene silencing treatment.

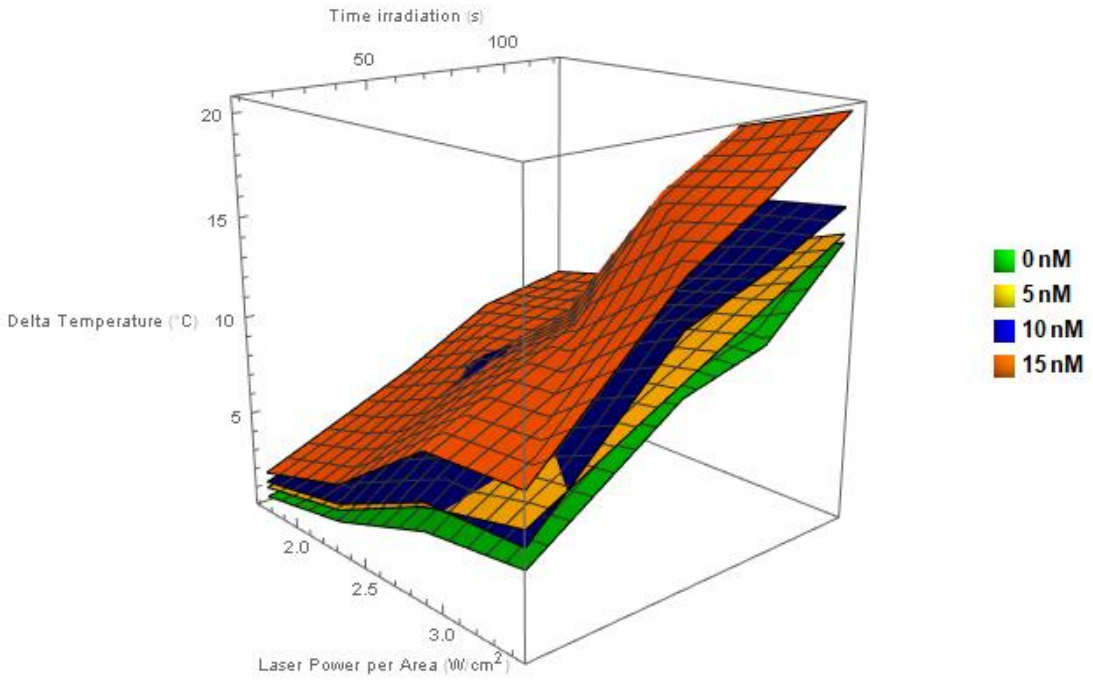


Figure 3.14: Representation of the hyperthermia system in a 3D graph. In this graph, it is possible to evaluate the impact of each variable (AuNP@30%PEG concentration, delta temperature and time, and laser irradiation). The variable that has the greatest impact is the AuNP@30%PEG concentration.

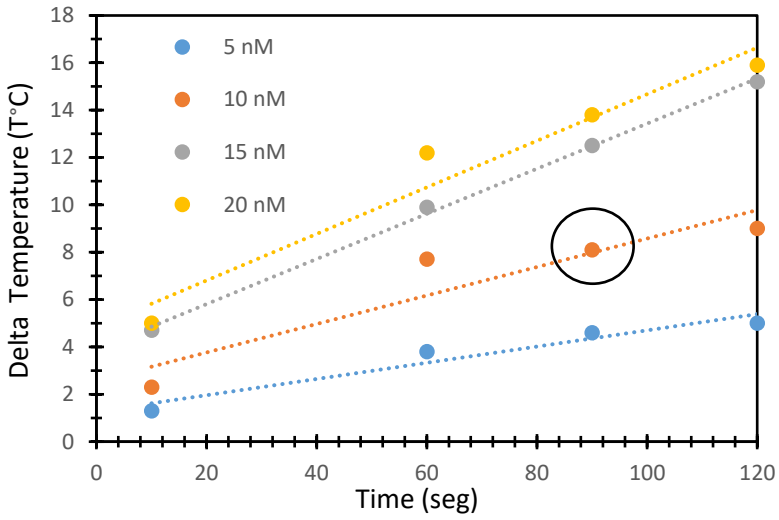


Figure 3.15: Linear function between irradiation time and the delta temperature registered on the 96 well-plate, with different AuNP@30%PEG concentrations. The concentrations used were 5 nM, 10 nM, 15 nM, and 20 nM from bot to top accordingly. The delta temperature was calculated by inferring the increment of temperature after irradiating the 96 well-plate since the hyperthermia regimen is within a specific temperature increment in the cells. From the increment of the HCT116 cells temperature with 10 nM of AuNP@30%PEG, it is possible to observe the laser power's impact, where only at 1.71 w/cm$^2$ the hyperthermia state is achieved after 90 s of irradiation.

## 3.5 AuNP characterization as photothermal agents

Upon irradiating a noble metal NP (e.g., gold, silver, copper) with external light at the appropriate wavelength, free electrons on the nanoparticle surface are excited, and conduction-free band electrons collectively oscillate at the same frequency. The transfer of energy of the SPR has several effects like photoemission, photochemistry, and local heating as a photothermal effect. The photothermal effect is where photon energy is converted into thermal energy by plasmonic materials, having a few energy losses other than heat dissipation for NPs upon irradiation [134].

In a hyperthermia system, it is essential to calculate the photothermal conversion of the AuNP and the heat generated by the particles upon irradiation to characterize them as photothermal agents further. For calculating the heat generated per particle, the thermal capacity of water 4.18 Jg$^{-1}$K$^{-1}$ (q) and the irradiated mass (m) of 0.2 g were used in Equation 4, where we calculate Q, the heat energy transferred in joules (J). $\Delta T$ is the temperature variation (calculated by subtracting the final temperature to the initial temperature in each nanoparticle assay, minus the variation in temperature for irradiating only water), q the water capacity and m the irradiated mass.

$$Q = q \times \Delta T \times m \qquad (4)$$

The number of nanoparticles was calculated using Beer-Lambert law with an ε = $2.85\times10^{-8}$ $M^{-1}$ $cm^{-1}$ at 520 nm for 14 nm diameter nanoparticles, according to Navarro et al. [135] and Avogadro number. Then, by dividing the total heat generated per assay by the number of particles and by the irradiation time (90 s), it was obtained a photothermal power of $4\times10^{-13}$ $J.s^{-1}$ per particle (figure 3.16-a)).

Regarding the laser intensity, the light energy that gets to each sample is equal to the number of photons arriving during irradiation, multiplied by each photon's energy. However, it is crucial to notice that not all energy is absorbed by the sample. As such, it was first determined the absorbed intensity fraction of the laser, using Equation 5 that allows calculating the intensity absorbed fraction of laser (IA), where I0 is the irradiated intensity of the laser source and A is the absorption at the irradiated wavelength.

$$IA = I0 \times (1 - 10^{-A}) \qquad (5)$$

Overall, the AuNP have a photothermal conversion of 71% as shown in figure 3.16-b). For 5 and 10 nM, the AuNP@30%PEG have a photothermal conversion of 77% (figure 3.16-b)), quite similar compared to the literature that projected efficiency of 78 % for citrate capped 15.7 nm AuNP [123].

This proves that the photoconversion is affected by the concentration. The fact that the conversion is dependent on the concentrations may be due to the high concentration of AuNP. The AuNP concentration causes the effect of an inner filter, where the sample is not heated homogeneously. In this case, only the surface AuNP is excited by the laser irradiation generating more heat than the ones underneath [136]. Another aspect aside from the inner filter effect caused by the AuNP is the heterogeneous irradiation on the well since the heat generated will be more intense in the centre than in the well's surroundings.

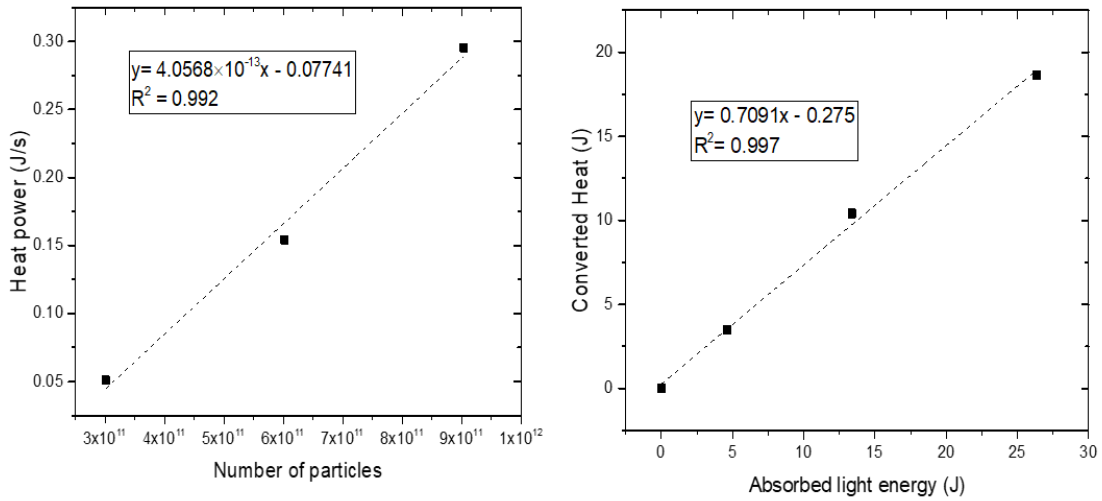


Figure 3.16: Characterization of the Photothermal effect of the AuNP@30%PEG. On the left a), the heat generated per second in the function of the number of particles after laser irradiation of 1.71 W/cm$^2$ for 90 s. On the right b), the photothermal conversion efficiency of 14 nm AuNP.

The photothermal effect is greatly enhanced under plasmon resonance, due to the photoconversion capacity of the NPs to convert the transfer photon energy of the light absorbed by the laser irradiation into heat. AuNPs are excellent for photoconversion with efficient plasmon absorption in the visible and NIR regions since they present photostability, low luminescence yield, and rapid relaxation of the SPR [68].

The capacity for the light-to-heat conversion is not directly predicted by the optical absorption spectrum since it depends on parameters such as size and concentration. The concentration of the AuNP is related to the inner filter effect that the NP cause on heat distribution on the sample. In terms of size, according to Mie theory, larger NPs have more scattering than absorption [123], [137]. The plasmon resonance wavelengths are significantly less optically tuneable compared to NPs with a larger diameter. Therefore, smaller NPs have higher efficiencies due to their higher abs/ext ratios having a lower heat dissipation.

## 3.6 Cell viability assays

Cell viability is an essential factor in hyperthermia since it gives information about the biological response. The main objective is to make the cells more thermosensitive, thus increasing the treatment efficiency in cancer therapy [133]. The two methods used to access the cell viability were staining and colorimetric methods (Trypan blue and MTS,

respectively). As stated before, the Trypan blue method is a dye used to discriminate cells that have their cell membrane damaged selectively. The determination of membrane integrity is performed by dye exclusion straightforwardly and inexpensively. The drawback is that this technique depends on the operator, and it does not relate directly to the viability of the cell. MTS is a colorimetric method based on the quantification of the formazan produced by the cells. This method is directly related to the metabolic activity translated by the increase of absorbance; however, the absorbance is highly influenced by the incubation time, cell type, and cell number.

The cell viability assays were normalized with HCT-116 cells without laser irradiation or AuNPs. The calculation for the cell viability was performed using Equation 1 from section 2.7. In the Trypan blue assay, the cells irradiated with AuNP present a lower cell viability (3.17), having a statistically significant difference compared to the control (HCT116 cells). This value is translated in the number of cells that have the cell membrane damaged, possibly due to the heat generated by the AuNP internalized after laser irradiation. Since the Trypan blue assay is a staining method that will discriminate between cells with the cell membrane compromised, it is plausible to assume that the cells irradiated with AuNP have the cell membrane permeability more affected.

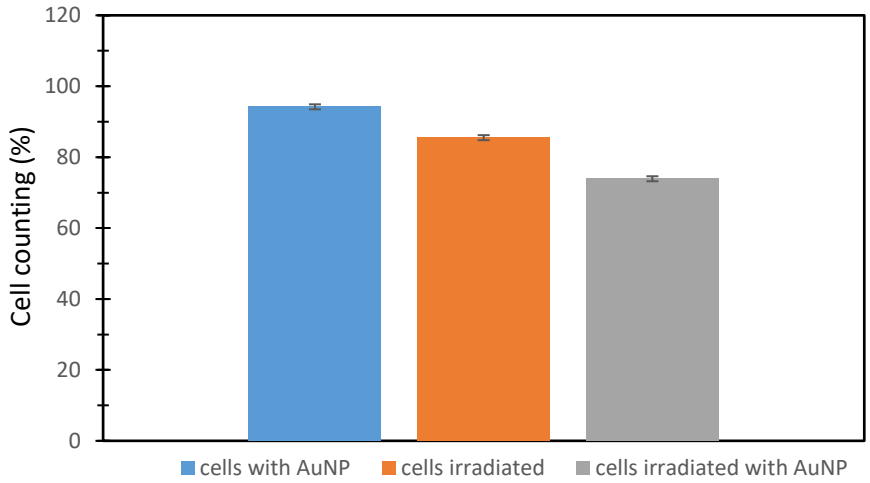


Figure 3.17: Trypan blue assay with a concentration of 10 nM AuNP@30%@PEG, irradiated with laser irradiation of 1.71 W/cm$^2$ for 90 s. The assay shows a difference in the cells irradiated with AuNP, compared to the cells with AuNP and the cells irradiated. This fact may be due to the heat generated by the AuNP when irradiated with the green laser in the same wavelength of the NPs (~532nm).

In figure 3.18, it is possible to the MTS assay results of each condition tested (AuNP, laser irradiation, and AuNP + laser irradiation). The cells irradiated with AuNP have a statistically significant decrease in cell viability, with a reduction of approximately 5%, compared to the control (HCT116 cells).

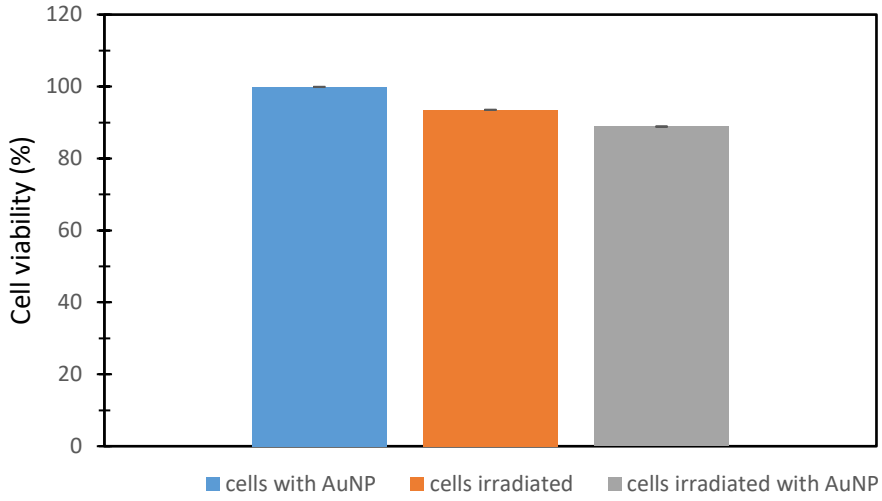


Figure 3.18: MTS assay with a concentration of 10 nM of AuNP@30%PEG, irradiated with laser irradiation of 1.71 W/cm$^2$ for 90 s. In the MTS assay, the difference in the cell viability is not very predominant in the cells irradiated with AuNP, possibly due to the HCT116 cells remain their ability to remain active while other cellular components (e.g., cell membrane) may be more affected by the AuNP and irradiation.

By comparing the MTS and Trypan blue results, it is possible to observe a discrepancy between the cell viability results. These results corroborate the idea that the membrane is damaged while the cells stayed metabolically active after laser irradiation. It is plausible to assume that the hyperthermia achieved (with 10 nM of AuNP@30%PEG irradiated with a laser current of 3.12 mA for 90 s) induces an alteration of the cell permeability, due to the heat generated by the AuNP that may be in the medium or within the tumour cells. The cell permeability changes may be useful for combinatory approaches, where the enhanced cellular uptake increases the treatment's efficiency.

## 3.7 Effect of the variation of the AuNP concentration

The AuNP concentration is a crucial factor in PTT to ensure that the treatment is efficient with minimal side effects. As such, cell viability assays (Trypan blue and MTS) were performed to better understand the impact of the AuNP concentration on cell viability.

In figure 3.19 it is possible to observe the impact of the AuNP@30%PEG concentration on the cell viability of the HCT116 cells. At low concentrations (<5 nM) there is a difference between the cell viability assays. However, at 10 nM there is a noticeable discrepancy between the Trypan blue and MTS as previously addressed in section 3.6. At higher concentrations, the cell viability reduces, with signs of aggregation of the NPs in the cells after laser irradiation.

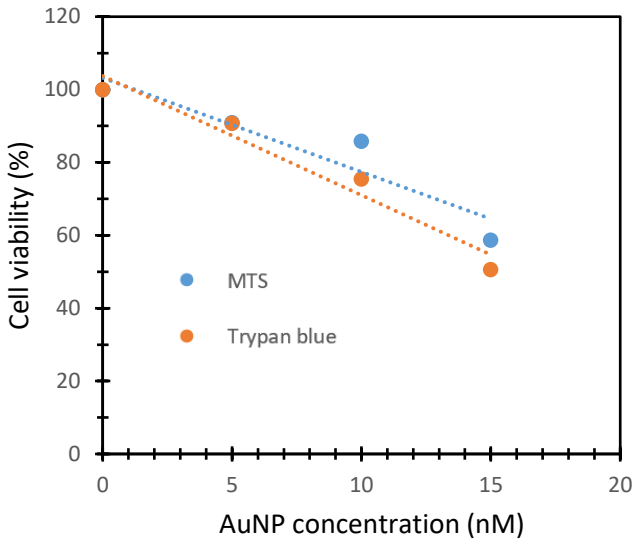


Figure 3.19: Correlation between cell viability, tested with MTS and Trypan blue (represented by blue and orange colours, respectively), and AuNP@30%PEG concentration from 0-15 nM. The HCT116 cells were challenged with the AuNP and irradiated with laser irradiation of 1.71 W/cm$^2$ for 90 s.

The key points in PTT efficacy are mainly focused on the concentration of NPs, toxicity, circulation time and subcellular location of the NPs. In terms of the concentration parameter, there is a certain threshold between toxicity and effect, where at high concentration there is a higher probability of aggregation and at low concentration there is not sufficient NPs to produce the desire therapeutic effect [138]. As a result, it is important to define a therapeutic window regarding the PTT mediated with NPs. The surface treatment of the NP is also very relevant because it affects the heat generated by the AuNP. The core of the AuNPs acts as a heat-to-light conversion agent and the peripheral part is responsible for the NP stability in a physiological environment [139].

The discrepancy between the MTS and Trypan blue assays, on the cell viability and cell membrane integrity, evidence of the alteration of the cell permeability on the cancer cells. As a result, it is possible to assume that the heat generated was enough to enhance

the cellular uptake, enhancing the cell permeability. If the photothermal treatment is conducted by continuous wave laser, like the one used during this work, the AuNPs usually localized in the cytoplasm are more effective in inducing cell destruction than AuNPs localized at the nucleus [140]. As such, it is crucial to analyse the location of the AuNP in the cells to further understand the impact of the heat generated by the NPs on the cells.

## 3.8 ICP-AES

To further evaluate the cellular uptake and cell permeability, ICP-AES was performed to quantify the AuNP internalized by the cells. The analysis laboratory's contracted service performed the ICP-AES at the service of Academy and Industry - Chemistry Department FCT-NOVA. This analytical technique is used to detect chemical elements, quantifying the metal compounds (Au) within the sample. Two types of samples were taken (supernatant and cellular pellet) with and without irradiation. With these, it is possible to infer if the effect of the AuNP, whether it is more prominent outside (medium) or inside the cells. Figure 6.1 in Annex A shows the AuNP quantification by ICP-AES results with a calibration curve of different Au concentrations [mg/L]. The values were converted to % using as control the initial AuNP@30%PEG working solution of 10 nM used for the hyperthermia assay (Annex C- figure 5.1) to have a more precise calculation of Au's quantification.

ICP-AES protocol requires a large amount of the sample to minimize the errors in the quantification of Au. Since this experiment was optimized for a 96 well plate, there are some losses in volume affecting Au concentration. It is essential to point out that the cellular suspension has a ~20% concentration than the [Au] initial. The variation of Au in the pellet samples with and without irradiation indicates that the cells after laser irradiation have a change in the cell permeability. The cells with irradiation have a higher concentration of Au of around ~0.009436 mg/L, suggesting that the hyperthermia improves the cellular uptake of the AuNP (see Table 3.1).

This increase in the cellular uptake may be explained by some studies performed, where it was demonstrated the optimization of the cell permeability upon irradiation with a visible light laser. As stated in the literature, it was reported the membrane permeabilization of adherently growing ovarian carcinoma cells (OVCAR-3) after irradiated with a green laser (532 nm) [141].

Table 3.1: Representation of the [Au] calculated for each sample to infer the Au internalized by the HCT116 cells.

| Samples | % | Au [mg/l) |
|---|---|---|
| AuNP initial solution | 100.0 | 0.6070 |
| Cellular Suspension | 20.11 | 0.1221 |
| Pellet | 0.1439 | 0.0008737 |
| Pellet with irradiation | 1.555 | 0.009436 |

Cellular uptake of AuNPs is essential for PTT mediated with NPs, where the therapeutic effects depend on the NPs cellular location. AuNPs can either remain on the cell surface or induce biological responses through different cellular uptake pathways. While the cell membrane is the main barrier for the NPs to enter into the cells, damaging the cell membrane through the PTT is proven to be a non-invasive and irreversible technique for destroying the cancer cells [139], [142].

The use of continuous wave laser irradiation for PTT mediated with NPs, shown to be more effective when the NPs are in the cell membrane. By damaging the cell membrane the NPs alter the cell permeability, enhancing the cellular uptake of therapeutic agents [138], [143]. Perfusion and oxygenation of tissues are also favoured by moderate heating, which may justify the use of AuNPs for photothermal improvement of cellular delivery. As a result, hyperthermia shows to be a potential treatment that uses the increment of temperature on the cells to affect the cell membrane's permeabilization and affects the tumour cell´s death.

The AuNPs can be considered as a mass-spring harmonic oscillator driven by the energy resonant light wave, therefore the increment of temperature occurs more intensively at the surface of the NP. However, it is important to notice that there is an amount of energy that is transferred to the medium. The heating of the AuNPs in the medium is also a way to control and guide the NPs to specific locations, with the addition that heating the medium may be more effective than the cells [144], [145].

## 3.9 Cell viability assay of the combinatory approach (PTT and gene silencing)

After confirming and characterizing the hyperthermia, it was then possible to combine it with the silencing of *c-MYC*. The protocol and functionalized AuNP for the silencing of *c-MYC* were performed by David Fontinha. The cell viability assays were performed in a 96-well plate with an inoculum of $2\times10^4$ HCT116 cells/well, with a concentration of 0.6 nM of AuNP@MYC irradiated with 1.71 W/cm$^2$ for 90 s.

Firstly, it is essential to understand the effect of the AuNP@30%PEG and AuNP@MYC on the cells. The cell viability performed was calculated by normalizing with normal HCT116 cells. The observed cell viability shown in figure 3.20 shows the AuNP increases the cells' metabolism, as previously mentioned in section 3.6. However, there is a significant difference between AuNP@30%PEG and AuNP@MYC, where it is possible to see the impact of the gene silencing of *c-MYC*. It was reported that the cells undergo some changes in the number of cytoplasmic organelles during the cellular uptake [146]. This fact may explain the high metabolic activity of the cells during this process in the cells with AuNP@PEG.

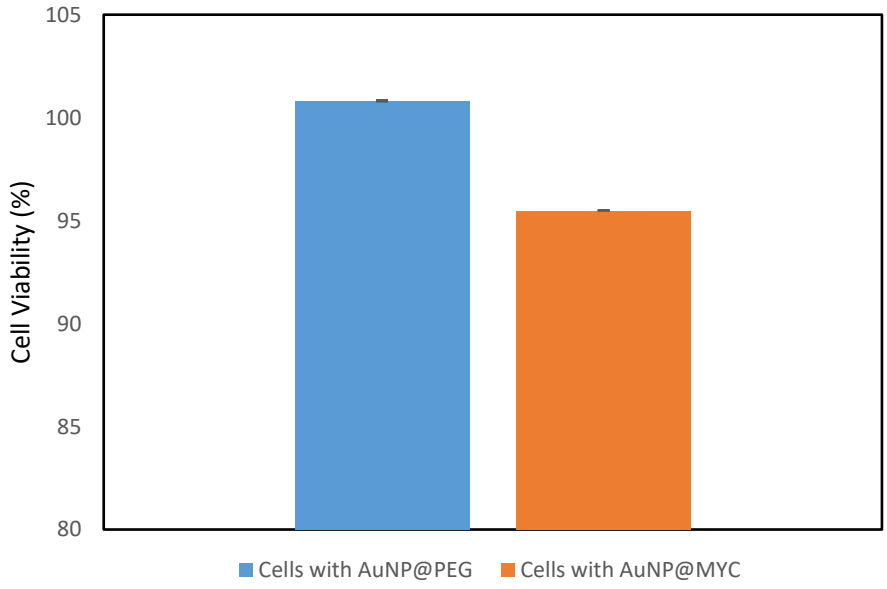


Figure 3.20: MTS assay from $2\times10^4$ HCT116 cells/well were seeded, challenged with 0.6 nM of AuNP@30%PEG and AuNP@MYC. The AuNP@30%PEG have higher cell viability (>100%) due to the cellular uptake of the NPs increase cell metabolism. The AuNP@MYC have a slight decrease in the cellular uptake, possibly because of the decrease in cell proliferation because of the silencing of *c-MYC*.

By considering the influence of the AuNP@MYC on the cells, it was then performed the cell viability assay with laser irradiation of 1.71 W/cm$^2$ for 90 s. The cell viability was normalized with HCT116 cells irradiated to evaluate the irradiation effects combined with the silencing of *c-MYC*. The cell viability shows that the laser irradiation is an evident influence, where AuNP@30%PEG shows a slight decrease in cell viability (figure 3.21). Nevertheless, the AuNP@30%PEG shows high cell viability since they are stable after irradiation showing low cytotoxicity. The AuNP@MYC presents a decrease of the cell viability, compared to AuNP@30%PEG irradiated. This decrease in viability can be explained by the combinatory approach of both gene silencing and hyperthermia, where the AuNP internalization was enhanced. These results are supported by the ICP-AES results, stated in section 3.8.

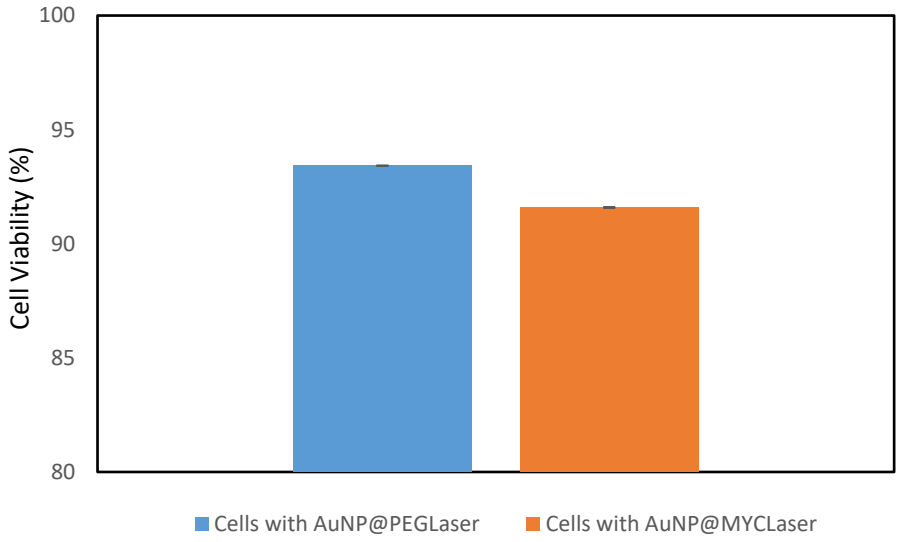


Figure 3.21: MTS assay was 2×10$^4$ HCT116 cells/well were seeded, challenged with 0.6 nM of AuNP@30%PEG, and AuNP@MYC and treated with laser irradiation of 1.71 W/cm$^2$ for 90 s. In this assay, the cell viability has a more predominant decrease, probably due to the irradiation and the heat generated by the NPs.

PTT is a minimally invasive treatment method based on the photothermal conversion of the AuNPs to induce hyperthermia. The AuNPs used in PTT are mainly composed of the core, which acts as the heat-to-light conversion agent, and the peripheral part that is responsible for the stability as well as loading targeting agents. Although the AuNPs can passively accumulate in the cancer cells, the uniform and efficient AuNPs cellular uptake is complex due to the biological interactions. This fact may be due to the non-specific targeting in PTT since it faces some challenges such the escape from specific

subcellular sites such as lysosome, endosome, and mitochondria [139], [143], [147], [148].

In result, the cell viability results support the use of PTT with visible light in this specific cell line (HCT116), altering the cell permeability in a non-lethal procedure with the purpose of being used in combinatory therapies.

## 3.10 Gene expression analysis

Gel electrophoresis is a process of separating biomolecules, based on their sizes, by running them through a gel-like matrix by using an electric field. Larger molecules move more slowly, while smaller molecules slip through the matrix and move faster and farther, thus separating the different fragments based on size. Depending on the biomolecules' weight, the agarose's weight varies since it involves the gel matrix's mesh size. High weight molecules need a lower % agarose, while small molecules need a higher % to run through the matrix gel [149].

Figure 3.22 shows the electrophoresis gel with the result of the amplification of the PCR products. Firstly, it is essential to analyse the controls used, the positive control (HCT116 genome), and the negative control is not amplified, meaning there are no signs of contamination. By comparing the DNA ladder and the samples, it is possible to visualize a band ~229 bp corresponded to the *c-MYC*. There may be a presence of dimers (second band below 100 bp), nevertheless, these bands are not significant since they are not so prominent as the rest of the bands. The samples from 1-4 with the *c-MYC* primers are feebler compared to the 5-8 bands that have the 18S primers. The 5-8 bands are more prominent due to the 18S constitutive gene expression. The band 3 and 4 corresponding to the AuNP@MYC, and AuNP@MYC@Laser respectively, also seem to be feebler compared to the 1 and 2 band corresponding to the AuNP@30%PEG, and AuNP@30%PEG respectively. In result, this indicates the potential silencing of the *c-MYC*.

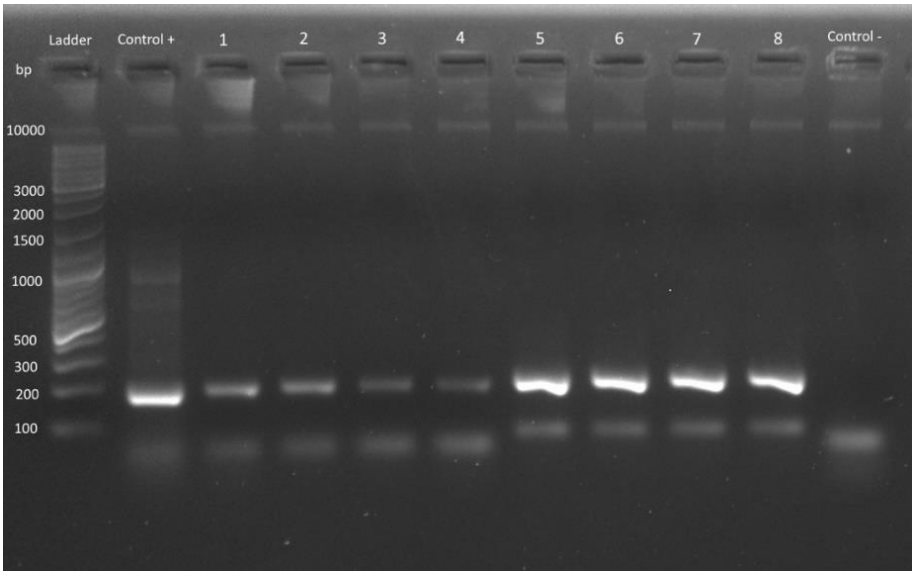


Figure 3.22: Image of the gel electrophoresis of 1.5 (w/v) during 45 min at 90 mV with the ladder (GeneRuler DNA Ladder Mix SM0331 (Thermo Scientific, Waltham, MA, USA)), positive control as the DNA genomic of HCT116 and the negative control without any DNA template. The samples from 1-4 (AuNP@30%PEG, AuNP@30%PEG@Laser, AuNP@MYC, and AuNP@MYC@Laser from left to right, respectively) are with *c-MYC* primers. The samples from 5-8 (AuNP@30%PEG, AuNP@30%PEG@Laser, AuNP@MYC, and AuNP@MYC@Laser from left to right, respectively) are with 18S primers.

The RT-qPCR provides information about the gene expression of the *c-MYC*, being essential combined with the cell viability assays, to evaluate the synergy between the gene silencing and laser irradiation on HCT116 cells. Firstly, it was evaluated the mRNA extracted, where it is possible to observe in figure 3.23 that the samples treated with irradiation show less amount of mRNA when compared to the cells with only AuNP@30%PEG and AuNP@MYC. The difference between the samples treated is more noticeable since the laser irradiation itself may enhance cell death or even detached the cell from the surface of the microplate. As such, the normalization of the data was performed dividing the samples with and without laser treatment (group 1 and 2 respectively) and using the mean in the analysis expression of the *c-MYC*.

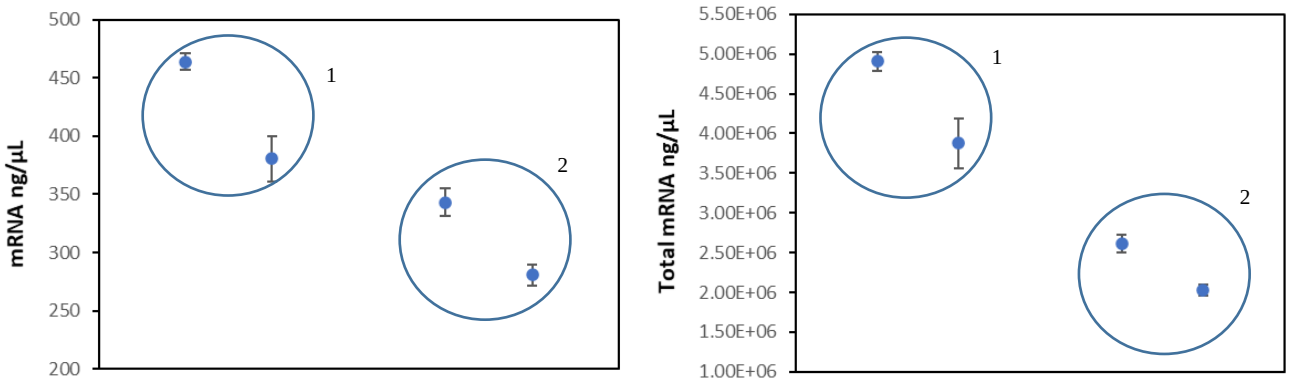


Figure 3.23: Results of the mRNA and total mRNA extracted in the HCT116 cells (from left to right AuNP@30%PEG, AuNP@MYC (group 1), AuNP@30%PEG@Laser, and AuNP@MYC@Laser (group 2), where it is possible to observe the effect of the laser irradiation in the mRNA.

Figure 3.24 shows the RT-qPCR results, using as control AuNP@30%PEG and AuNP@30%PEG@Laser, with a threshold defined for the Ct values has of 0.12. Since the laser affects the mRNA, the values were normalized considering the total mRNA extracted for each condition tested. The contrast between AuNP@30%PEG and AuNP@MYC (group 1) shows a statistically significant reduction of the *c-MYC* relative expression ~50% (the fold change of $2^{-\Delta\Delta ct}$ is approximately equal to 0.4). When comparing with the results in the literature where there is a reduction of the *c-MYC* gene relative expression of >60%, the gene silencing applied in this work did have indeed a successful efficiency in the gene silencing of *c-MYC* with an operational AuNP pegylated [150].

In figure 3.24, group 2 shows a reduction of almost 70% after applied the laser irradiation (the fold change of $2^{-\Delta\Delta ct}$ is approximately equal to 0.19). It is noticeable that the laser irradiation influences greatly the *c-MYC* expression, supported by the ICP-AES and cell viability results, where the laser irradiation enhances the permeability increasing the gene delivery in the cells. As such, the gene silencing was possibly enhanced since the increased cellular uptake due to the laser irradiation of the PTT treatment.

This significant reduction of the *c-MYC* relative gene expression, based on the irradiation of the cells with a laser may prove to be an alternative as a transfection method for gene delivery like lipofection or electroporation. The combination of the laser irradiation with AuNPs, as excellent vectors for gene delivery, evokes the transient cell membrane permeabilization through their SPR effect. As stated before, the SPR effect of the AuNPs is utilized to enhance the photothermal conversion and thus generate more localized heat, affecting the cell membrane permeabilization.

Studies demonstrate the use of AuNPs with visible light laser, for efficient transfection of siRNA without compromising the cell viability of the ZMTH3 cells [151]. The results obtained are in concordance with the following, where it was possible to obtain a higher gene silencing without damaging the cell viability (>90% in all conditions as shown in figure 3.22).

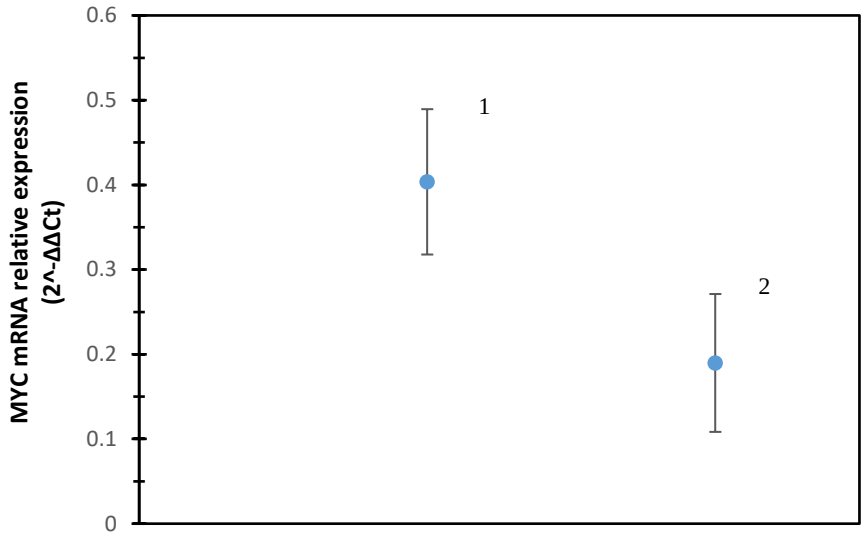


Figure 3.24: RT-qPCR results with the relative quantification of the mRNA expression of each condition tested from left to right it is represented group 1 from the previous normalization referring to the samples without laser treatment and group 2 the samples with laser treatment. The gene expression analysis shows an efficient gene silencing of around 50% without laser treatment and after laser irradiation the reduction of c-MYC was about 70%, indicating that after laser irradiation there is a higher reduction of the *c-MYC* expression.

# 4. Conclusion

This thesis proposed to study the combinatory effect of hyperthermia and gene silencing approach, to demonstrate the laser ablation of tumour cells in a controllable manner to further enhance the treatment efficacy.

It was synthesized and characterized the different types of AuNP to estimate the size and surface charge by UV-Vis, DLS, and ZP. The AuNP were subjected to different stability assays to ensure their resistance against different osmolarities and ionic forces, simulating a biological system. AuNP@PEG showed better stability, proving that PEG is an excellent capping agent.

The PTT system was characterized and optimized, obtaining a hyperthermia state on the HCT116 with 10 nM AuNP@30%PEG concentration for laser irradiation of 1.71 $W/cm^2$ for 90 s. The photoconversion obtained by the AuNP@30%PEG when irradiated with the laser, was highly efficient with a value of approximately 77%. Subsequently, the cell viability assays were performed to better define the hyperthermia effects since the heat may cause effects ranging from reversible to irreversible damages to the tumour cells. It is essential to consider some parameters that may induce some side effects in the cell viability such as the AuNP concentration (saturation of AuNPs on the cells with possible cytotoxic effects) and the irradiation itself (excess production of heat and instability of gene expression).

The cell viability assays showed a discrepancy between the TP and MTS assays, where it was made the hypothesis of the hyperthermia enhancing the permeability of the cells. It was further explained with the ICP-AES experiment, that a higher percentage of Au was inside the cells after irradiation. As a result, it was crucial to analyse the concentration of AuNP internalize by the cells to achieve hyperthermia, to further support the enhanced cellular uptake of the cells after irradiation.

By consolidating the AuNP photothermal characterization, the gene silencing was performed with the AuNP@MYC. It was showed that gene silencing occurs with an almost 50% reduction of the relative gene expression. When combined with the laser irradiation, there is a reduction of approximately 70% of the *c-MYC* gene relative expression.

PTT mediated with AuNP can sensitize cancer cells to gene silencing by increasing cell permeability and intracellular delivery. As such, the controlled release and hyperthermia-induced sensitization can lower the required therapy dosages thus increasing the efficacy of the treatment [152]. This work supports the potential use of hyperthermia as a

cooperative treatment, to enhance the cell permeability as well as demonstrates the potential use of AuNP for combinatory approaches, exploring the multifunctionality of the AuNP in PTT with green lasers (visible light), in epithelial cancers.

# 5. Future Perspectives

The theme proposed in this thesis, the combinatory approach of hyperthermia and gene therapy simultaneously, was innovative and quite challenging, which led to several optimizations in the course of the work, with some experiments taking longer than expected, as it was necessary to modify some existing protocols. On the other hand, during the execution of this work, COVID-19 appeared, which limited the practical realization of complementary experiences, which is why I present in what follows, a set of additional experiments that should be considered in future work.

### AuNP and AuNP-conjugates characterization

AuNP characterization is fundamental since it provides information about the physical, optical, and structural properties of the NPs. These properties are quite important since it affects the NPs behaviour *in vivo.* Concerning the size of the AuNPs, this was estimated through optical methods, nevertheless, to have a more rigorous measurement as well as surface composition, a more precise and powerful technique such as Transmission Electron Microscopy (TEM) should be used. TEM is an excellent tool for characterizing the size of NPs as well as the chemical composition not only in the bulk but also at the surface of the NPs, and this is quite important since could determine the type of functionalization to be used [153].

Another aspect to consider is the stability assays performed with the AuNP. The AuNP aggregation is intricately related to the SPR effect, an optical property of the NPs. It is the main responsible for the light-to-heat conversion in hyperthermia. To further examine the SPR, it is essential to look at the factors that influence the NP's size like temperature, pH, ionic force, and mechanical forces [90].

### Hyperthermia Characterization

In the hyperthermia system's characterization, it is essential to test more concentrations of AuNP to have a broader range of the AuNP in the therapeutic window for potential clinical applications. In terms of the AuNP characterization, it would be essential to analyse by DLS the AuNP size when subjected to the laser irradiation to observe a variation of the size of the NPs. These results would provide information about the effects of the laser irradiation on the SPR effect and size, interesting for the possibility to better understand the photoconversion of the AuNP.

### Cellular internalization of the NPs

In terms of nanotechnology applications, it is essential to notice the intracellular tracking of the NPs, which affects the therapeutic effect. As stated in the introduction, AuNPs uptake's most effective mechanism is the receptor-mediated endocytosis [49]. This process can also be called active transport, which can be delayed/inhibited by temperature. To better examine the internalization of the NPs, it would be interesting to evaluate the cellular uptake in different temperatures (37 ºC and -4 ºC). After analysis of the ICP-AES, it would be expected for fewer AuNP to be internalized at lower temperatures, supporting the mechanism of cellular internalization of the NPs [154].

### Flow Cytometry analysis

Flow cytometry analysis is based on the measurement of cell characteristics, allowing the characterization of individual cells. This analysis may provide interesting information about this cell line (HCT116) and, more importantly, about the cell death mechanism that the cells have with hyperthermia. In hyperthermia, the cell death mechanism expected is apoptosis [155]. The apoptosis may occur by protein damage, membrane damage, and cell proliferation. In this case, since the focus is to enhance the cells' permeability, it is essential to analyse the cell death mechanisms and quantify them properly.

# 6 References


[1] F. Bray, J. Ferlay, I. Soerjomataram, R. L. Siegel, L. A. Torre, and A. Jemal, "Global cancer statistics 2018: GLOBOCAN estimates of incidence and mortality worldwide for 36 cancers in 185 countries," *CA. Cancer J. Clin.*, vol. 68, no. 6, pp. 394–424, 2018.

[2] S. H. Hassanpour and M. Dehghani, "Review of cancer from perspective of molecular," *J. Cancer Res. Pract.*, vol. 4, no. 4, pp. 127–129, 2017.

[3] M. Topçul and İ. Çetin, "The Biology Of Cancer Metastasis," 2015, pp. 1–20.

[4] K. W. Hunter, N. P. S. Crawford, and J. Alsarraj, "Mechanisms of metastasis," *Breast Cancer Res.*, vol. 10, pp. 1–10, 2008.

[5] J. S. Bertram, "The molecular biology of cancer.," *Mol. Aspects Med.*, vol. 21, no. 6, pp. 167–223, 2000.

[6] H. F. Dvorak, L. F. Brown, M. Detmar, and A. M. Dvorak, "Vascular permeability factor/vascular endothelial growth factor, microvascular hyperpermeability, and angiogenesis.," *Am. J. Pathol.*, vol. 146, no. 5, pp. 1029–1039, 1995.

[7] B. R. Zetter, "Angiogenesis and tumour metastasis.," *Annu. Rev. Med.*, vol. 49, pp. 407–424, 1998.

[8] C. G. Drake, E. Jaffee, and D. M. B. T.-A. in I. Pardoll, "Mechanisms of Immune Evasion by Tumours," in *Cancer Immunotherapy*, vol. 90, Academic Press, 2006, pp. 51–81. [1] C. G. Drake, E. Jaffee, and D. M. B. T.-A. in I. Pardoll, "Mechanisms of Immune Evasion by Tumours," in *Cancer Immunotherapy*, vol. 90, Academic Press, 2006, pp. 51–81.

[9] E. J. Kuipers *et al.*, "Colorectal cancer.," *Nat. Rev. Dis. Prim.*, vol. 1, p. 15065, Nov. 2015.

[10] J. J. Granados-Romero *et al.*, "Colorectal cancer: a review," *Int. J. Res. Med. Sci.*, vol. 5, no. 11, p. 4667-76, 2017.

[11] R. Rampado, S. Crotti, P. Caliceti, S. Pucciarelli, and M. Agostini, "Nanovectors Design for Theranostic Applications in Colorectal Cancer," *J. Oncol.*, 2019.

[12] American Cancer Society, "Colorectal Cancer," 2019. [Online]. Available: https://www.cancer.org/cancer/colon-rectal-cancer/about/what-is-colorectal-cancer.html [Accessed: 20-Oct-2020].

[13] M. Arruebo *et al.*, "Assessment of the evolution of cancer treatment therapies," *Cancers (Basel).*, vol. 3, no. 3, pp. 3279–3330, 2011.

[14] I. Dagogo-Jack and A. T. Shaw, "Tumour heterogeneity and resistance to cancer therapies," *Nat. Rev. Clin. Oncol.*, vol. 15, no. 2, pp. 81–94, 2018.

[15] A. Urruticoechea, R. Alemany, J. Balart, A. Villanueva, F. Viñals, and G. Capellá, "Recent advances in cancer therapy: an overview.," *Curr. Pharm. Des.*, vol. 16, no. 1, pp. 3–10, Jan. 2010.

[16] J. Zugazagoitia, C. Guedes, S. Ponce, I. Ferrer, S. Molina-Pinelo, and L. Paz-Ares, "Current Challenges in Cancer Treatment," *Clin. Ther.*, vol. 38, no. 7, pp. 1551–

1566, 2016.

[17] J. Shi, P. W. Kantoff, R. Wooster, and O. C. Farokhzad, “Cancer nanomedicine: Progress, challenges and opportunities,” *Nat. Rev. Cancer*, vol. 17, no. 1, pp. 20–37, 2017.

[18] H. Chen *et al.*, “Precise nanomedicine for intelligent therapy of cancer,” *Sci. China Chem.*, vol. 61, no. 12, pp. 1503–1552, 2018.

[19] S. Tran, P.-J. DeGiovanni, B. Piel, and P. Rai, “Cancer nanomedicine: a review of recent success in drug delivery,” *Clin. Transl. Med.*, vol. 6, no. 1, 2017.

[20] J. Conde, J. Rosa, J. C. Lima, and P. V Baptista, “Nanophotonics for Molecular Diagnostics and Therapy Applications,” *Int. J. Photoenergy*, vol. 2012, p. 1-11, 2012.

[21] I. I. Lungu, A. M. Grumezescu, A. Volceanov, and E. Andronescu, “Nanobiomaterials Used in Cancer Therapy: An Up-To-Date Overview,” *Molecules*, vol. 24, no. 19. 2019.

[22] A. Carvalho, A. R. Fernandes, and P. V Baptista, “Chapter 10 - Nanoparticles as Delivery Systems in Cancer Therapy: Focus on Gold Nanoparticles and Drugs,” in *Micro and Nano Technologies*, S. S. Mohapatra, S. Ranjan, N. Dasgupta, R. K. Mishra, and S. B. T.-A. of T. N. D. and D. S. Thomas, Eds. Elsevier, 2019, pp. 257–295.

[23] P. N. Navya, A. Kaphle, S. P. Srinivas, S. K. Bhargava, V. M. Rotello, and H. K. Daima, “Current trends and challenges in cancer management and therapy using designer nanomaterials,” *Nano Converg.*, vol. 6, no. 1, p. 1-23, 2019.

[24] Y. Fukumori and H. Ichikawa, “Nanoparticles for cancer therapy and diagnosis,” *Adv. Powder Technol.*, vol. 17, no. 1, pp. 1–28, 2006.

[25] D. Ferreira, D. Fontinha, C. Martins, D. Pires, A. R. Fernandes, and P. V. Baptista, “Gold Nanoparticles for Vectorization of Nucleic Acids for Cancer Therapeutics,” *Molecules*, vol. 25, no. 15, 2020.

[26] E. Abbasi *et al.*, “Dendrimers: synthesis, applications, and properties,” *Nanoscale Res. Lett.*, vol. 9, no. 1, p. 1-247, May 2014.

[27] F. U. Din *et al.*, “Effective use of nanocarriers as drug delivery systems for the treatment of selected tumours,” *Int. J. Nanomedicine*, vol. 12, pp. 7291–7309, 2017.

[28] A. Akbarzadeh *et al.*, “Liposome: classification, preparation, and applications.,” *Nanoscale Res. Lett.*, vol. 8, no. 1, p. 1-102, Feb. 2013.

[29] H. Pandey, R. Rani, and V. Agarwal, “Liposome and Their Applications in Cancer Therapy,” *Brazilian Arch. Biol. Technol.*, vol. 59, 2016.

[30] J. M. Morachis, E. A. Mahmoud, and A. Almutairi, “Physical and Chemical Strategies for Therapeutic Delivery by Using Polymeric Nanoparticles,” *Pharmacol. Rev.*, vol. 64, no. 3, pp. 505– 519, Jul. 2012.

[31] J. H. Park, S. Lee, J. H. Kim, K. Park, K. Kim, and I. C. Kwon, “Polymeric nanomedicine for cancer therapy,” *Prog. Polym. Sci.*, vol. 33, no. 1, pp. 113–137, 2008.

[32] J. Saleem, L. Wang, and C. Chen, “Carbon-Based Nanomaterials for Cancer Therapy via Targeting Tumour Microenvironment,” *Adv. Healthc. Mater.*, vol. 7, no. 20, pp. 1–30, 2018.

[33] S. C. Ray and N. R. Jana, “Chapter 5 - Application of Carbon-Based Nanomaterials as Drug and Gene Delivery Carrier,” in *Micro and Nano Technologies*, S. C. Ray and N. R. B. T.-C. N. for B. and M. A. Jana, Eds. Elsevier, 2017, pp. 163–203.

[34] F.-G. Wu *et al.*, “Quantum Dots for Cancer Therapy and Bioimaging - Nanooncology: Engineering nanomaterials for cancer therapy and diagnosis,” G. Gonçalves and G. Tobias, Eds. Cham: Springer International Publishing, 2018, pp. 89–135.

[35] H. Zhang, D. Yee, and C. Wang, “Quantum dots for cancer diagnosis and therapy: Biological and clinical perspectives,” *Nanomedicine*, vol. 3, no. 1, pp. 83–91, 2008.

[36] A. Martinez-Finkelshtein and W. Van Assche, “Gold Nanoparticles: Preparation, Properties, and Applications in Bionanotechnology,” *Not. Am. Math. Soc.*, vol. 63, no. 09, pp. 1029–1031, 2016.

[37] S. Kumar *et al.*, “Functionalized gold nanostructures: Promising gene delivery vehicles in cancer treatment,” *RSC Adv.*, vol. 9, no. 41, pp. 23894–23907, 2019.

[38] A. Hervault and N. T. K. Thanh, “Magnetic nanoparticle-based therapeutic agents for thermo-chemotherapy treatment of cancer,” *Nanoscale*, vol. 6, no. 20, pp. 11553–11573, 2014.

[39] M. Wu and S. Huang, “Magnetic nanoparticles in cancer diagnosis, drug delivery and treatment.,” *Mol. Clin. Oncol.*, vol. 7, no. 5, pp. 738–746, 2017.

[40] R. Sinha, G. J. Kim, S. Nie, and D. M. Shin, “Nanotechnology in cancer therapeutics: bioconjugated nanoparticles for drug delivery,” *Mol. Cancer Ther.*, vol. 5, no. 8, pp. 1909–1917, 2006.

[41] A. Albanese, P. S. Tang, and W. C. W. Chan, “The Effect of Nanoparticle Size, Shape, and Surface Chemistry on Biological Systems,” *Annu. Rev. Biomed. Eng.*, vol. 14, no. 1, pp. 1–16, 2012.

[42] E. Pavitra *et al.*, “Engineered nanoparticles for imaging and drug delivery in colorectal cancer,” *Semin. Cancer Biol.*, vol. 69, pp. 293–306, 2021.

[43] Z. Zhang and M. R. King, “Nanomaterials for the Capture and Therapeutic Targeting of Circulating Tumour Cells,” *Cell. Mol. Bioeng.*, vol. 10, no. 4, pp. 275–294, 2017.

[44] L. Salvioni, M. A. Rizzuto, J. A. Bertolini, L. Pandolfi, M. Colombo, and D. Prosperi, “Thirty Years of Cancer Nanomedicine: Success, Frustration, and Hope,” *Cancers*, vol. 11, no. 12. 2019.

[45] N. D. Donahue, H. Acar, and S. Wilhelm, “Concepts of nanoparticle cellular uptake, intracellular trafficking, and kinetics in nanomedicine,” *Adv. Drug Deliv. Rev.*, vol. 143, pp. 68–96, 2019.

[46] X. M. Jiang, L. M. Wang, and C. Y. Chen, “Cellular uptake, intracellular trafficking and biological responses of gold nanoparticles,” *J. Chinese Chem. Soc.*,

vol. 58, no. 3, pp. 273–281, 2011.

[47] F. Zhao, Y. Zhao, Y. Liu, X. Chang, C. Chen, and Y. Zhao, "Cellular uptake, intracellular trafficking, and cytotoxicity of nanomaterials," *Small*, vol. 7, no. 10, pp. 1322–1337, 2011.

[48] R. S. Darweesh, N. M. Ayoub, and S. Nazzal, "Gold nanoparticles and angiogenesis: molecular mechanisms and biomedical applications.," *Int. J. Nanomedicine*, vol. 14, pp. 7643–7663, 2019.

[49] P. Decuzzi and M. Ferrari, "The role of specific and non-specific interactions in receptor-mediated endocytosis of nanoparticles," *Biomaterials*, vol. 28, no. 18, pp. 2915–2922, 2007.

[50] G. Doria *et al.*, "Noble metal nanoparticles for biosensing applications.," *Sensors (Basel).*, vol. 12, no. 2, pp. 1657–1687, 2012.

[51] S. Alex and A. Tiwari, "Functionalized gold nanoparticles: Synthesis, properties and applications-A review," *J. Nanosci. Nanotechnol.*, vol. 15, no. 3, pp. 1869–1894, 2015.

[52] P. Singh, S. Pandit, V. R. S. S. Mokkapati, A. Garg, V. Ravikumar, and I. Mijakovic, "Gold Nanoparticles in Diagnostics and Therapeutics for Human Cancer," *Int. J. Mol. Sci.*, no. 7, 2018.

[53] Z. Z. J. Lim, J. E. J. Li, C. T. Ng, L. Y. L. Yung, and B. H. Bay, "Gold nanoparticles in cancer therapy," *Acta Pharmacol. Sin.*, vol. 32, no. 8, pp. 983–990, 2011.

[54] J. D. O. de C. Conde, "Cancer theranostics: Multifunctional gold nanoparticles for diagnostics and therapy," Universidade NOVA de Lisboa (Portugal), 2013.

[55] P. Baptista *et al.*, "Gold nanoparticles for the development of clinical diagnosis methods.," *Anal. Bioanal. Chem.*, vol. 391, no. 3, pp. 943–950, 2008.

[56] N. M. N. Khairunisak Abdul Razak, Siti Rabizah Makhsin, Nor Dyana Zakaria, "Gold nanoparticles for diagnostic development," *Sustain. Diagnostics Low Resour. Areas*, p. 1-52, 2019.

[57] M. Cordeiro, F. F. Carlos, P. Pedrosa, A. Lopez, and P. V. Baptista, "Gold nanoparticles for diagnostics: Advances towards points of care," *Diagnostics*, vol. 6, no. 4, p. 1-20, 2016.

[58] B. Pelaz *et al.*, "Surface Functionalization of Nanoparticles with Polyethylene Glycol: Effects on Protein Adsorption and Cellular Uptake," *ACS Nano*, vol. 9, no. 7, pp. 6996–7008, 2015.

[59] J. V Jokerst, T. Lobovkina, R. N. Zare, and S. S. Gambhir, "Nanoparticle PEGylation for imaging and therapy," *Nanomedicine (Lond).*, vol. 6, no. 4, pp. 715–728, Jun. 2011.

[60] L. Torrisi and N. Restuccia, "Laser-Generated Au Nanoparticles for Bio-Medical Applications," *IRBM*, vol. 1, pp. 1–6, 2018.

[61] D. F. Costa, L. P. Mendes, and V. P. Torchilin, "The effect of low- and high-penetration light on localized cancer therapy," *Adv. Drug Deliv. Rev.*, vol. 138, pp. 105–116, 2019.

[62] D. C. Thang, Z. Wang, X. Lu, and B. Xing, “Precise cell behaviors manipulation through light-responsive nano-regulators: Recent advance and perspective,” *Theranostics*, vol. 9, no. 11, pp. 3308–3340, 2019.

[63] E. Schena, P. Saccomandi, and Y. Fong, “Laser Ablation for Cancer: Past, Present and Future,” *J. Funct. Biomater.*, vol. 8, no. 2, p. 19, 2017.

[64] D. Gao *et al.*, “Multifunctional phototheranostic nanomedicine for cancer imaging and treatment,” *Mater. Today Bio*, vol. 5, no. 100035, p. 1-33, 2020.

[65] J. Lin, K. Chen, and H. Liu, “Progress of nanotechnology for phototherapy : Fundamentals and applications,” vol. 4, no. 1, pp. 101–107, 2017.

[66] J. Chen *et al.*, “Nanomaterials as photothermal therapeutic agents,” *Prog. Mater. Sci.*, vol. 99, pp. 1–26, 2019.

[67] B. Seo *et al.*, “Small gold nanorods-loaded hybrid albumin nanoparticles with high photothermal efficacy for tumour ablation,” *Colloids Surfaces B Biointerfaces*, vol. 179, pp. 340–351, 2019.

[68] C. Yao *et al.*, “Gold Nanoparticle Mediated Phototherapy for Cancer,” *J. Nanomater.*, vol. 2016, pp. 1–29, 2016.

[69] K. König, “Multiphoton microscopy in life sciences,” *J. Microsc.*, vol. 200, no. 2, pp. 83–104, Nov. 2000.

[70] L. A. Austin, M. A. Mackey, E. C. Dreaden, and M. A. El-Sayed, “The optical, photothermal, and facile surface chemical properties of gold and silver nanoparticles in biodiagnostics, therapy, and drug delivery,” *Arch. Toxicol.*, vol. 88, no. 7, pp. 1391–1417, 2014.

[71] Y. Yan *et al.*, “Use of Lasers in Laryngeal Surgery,” *J. Voice*, vol. 24, no. 1, pp. 102–109, 2010.

[72] Z. Li *et al.*, “Recent Advances in Nanomaterials-Based Chemo-Photothermal Combination Therapy for Improving Cancer Treatment.,” *Front. Bioeng. Biotechnol.*, vol. 7, p. 1-293, 2019.

[73] A. Bettaieb, P. K. Wrzal, and D. Averill-Bates, “Hyperthermia: Cancer Treatment and Beyond,” in *Cancer Treatment - Conventional and Innovative Approaches*, L. Rangel, Ed. 2013, pp. 1–29.

[74] D. K. Chatterjee, P. Diagaradjane, and S. Krishnan, “Nanoparticle-mediated hyperthermia in cancer therapy,” *Ther. Deliv.*, vol. 2, no. 8, pp. 1001–1014, 2011.

[75] Y. Yagawa, K. Tanigawa, Y. Kobayashi, and M. Yamamoto, “Cancer immunity and therapy using hyperthermia with immunotherapy, radiotherapy, chemotherapy, and surgery,” *J. Cancer Metastasis Treat.*, vol. 3, pp. 218–230, 2017.

[76] N. S. Abadeer and C. J. Murphy, “Recent Progress in Cancer Thermal Therapy Using Gold Nanoparticles,” *J. Phys. Chem. C*, vol. 120, no. 9, pp. 4691–4716, 2016.

[77] Z. Ashikbayeva, D. Tosi, D. Balmassov, E. Schena, P. Saccomandi, and V. Inglezakis, “Application of Nanoparticles and Nanomaterials in Thermal Ablation Therapy of Cancer.,” *Nanomater. (Basel, Switzerland)*, vol. 9, no. 9, 2019.

[78] M. I. Khot, H. Andrew, H. S. Svavarsdottir, G. Armstrong, A. J. Quyn, and D. G. Jayne, “A Review on the Scope of Photothermal Therapy–Based Nanomedicines in Preclinical Models of Colorectal Cancer,” *Clin. Colorectal Cancer*, vol. 18, no. 2, pp. 200–209, 2019.

[79] R. M. Cabral and P. V. Baptista, “The chemistry and biology of gold nanoparticle-mediated photothermal therapy: promises and challenges,” *Nano Life*, vol. 3, no. 3, pp. 1–18, 2013.

[80] X. Xue *et al.*, “Trojan Horse nanotheranostics with dual transformability and multifunctionality for highly effective cancer treatment,” *Nat. Commun.*, vol. 9, no. 1, pp. 1–15, 2018.

[81] A. L. B. Seynhaeve, M. Amin, D. Haemmerich, G. C. van Rhoon, and T. L. M. ten Hagen, “Hyperthermia and smart drug delivery systems for solid tumour therapy,” *Adv. Drug Deliv. Rev.*, vol. 163–164, pp. 125–144, 2020.

[82] W. Fridman *et al.*, “The Immune Microenvironment: A Major Player in Human Cancers,” *Int. Arch. Allergy Immunol.*, vol. 164, pp. 13–26, May 2014.

[83] S. Annamaneni, S. K. Vishwakarma, P. B. Meka, A. A. Khan, and P. Nallari, “Regulation of heat shock protein-70 gene transcripts in breast cancer cells during hypo and hyperthermia exposure,” *Meta Gene*, vol. 20, no. 100548, pp. 1–9, 2019.

[84] B. A. Chabner and T. G. Roberts, “Chemotherapy and the war on cancer,” *Nat. Rev. Cancer*, vol. 5, no. 1, pp. 65–72, 2005.

[85] V. Schirrmacher, “From chemotherapy to biological therapy: A review of novel concepts to reduce the side effects of systemic cancer treatment (Review).,” *Int. J. Oncol.*, vol. 54, no. 2, pp. 407–419, Feb. 2019.

[86] E. Ricevuto, G. Bruera, and P. Marchetti, “General principles of chemotherapy,” *Eur. Rev. Med. Pharmacol. Sci.*, vol. 14, pp. 269–271, Apr. 2010.

[87] G. Pilkington, A. Boland, T. Brown, J. Oyee, A. Bagust, and R. Dickson, “A systematic review of the clinical effectiveness of first-line chemotherapy for adult patients with locally advanced or metastatic non-small cell lung cancer,” *Thorax*, vol. 70, no. 4, pp. 359–367, 2015.

[88] J. V. McGowan, R. Chung, A. Maulik, I. Piotrowska, J. M. Walker, and D. M. Yellon, “Anthracycline Chemotherapy and Cardiotoxicity,” *Cardiovasc. Drugs Ther.*, vol. 31, no. 1, pp. 63–75, 2017.

[89] A. G. Waks and E. P. Winer, “Breast Cancer Treatment: A Review.,” *JAMA*, vol. 321, no. 3, pp. 288–300, Jan. 2019.

[90] J. Beik *et al.*, “Gold nanoparticles in combinatorial cancer therapy strategies,” *Coord. Chem. Rev.*, vol. 387, pp. 299–324, 2019.

[91] R. Mendes, A. R. Fernandes, and P. V. Baptista, “Gold nanoparticle approach to the selective delivery of gene silencing in cancer-The case for combined delivery?,” *Genes (Basel).*, vol. 8, no. 3, 2017.

[92] C. Liu and N. Zhang, “Nanoparticles in Gene Therapy: Principles, Prospects, and Challenges,” in *Nanoparticles in Translational Science and Medicine*, vol. 104, A. B. T.-P. in M. B. and T. S. Villaverde, Ed. Academic Press, 2011, pp. 509–562.

[93] Y. Xin, M. Huang, W. W. Guo, Q. Huang, L. Z. Zhang, and G. Jiang, “Nano-based delivery of RNAi in cancer therapy.,” *Mol. Cancer*, vol. 16, no. 1, p. 1-134, 2017.

[94] J. Singh, H. Kaur, A. Kaushik, and S. Peer, “A review of antisense therapeutic interventions for molecular biological targets in various diseases,” *Int. J. Pharmacol.*, vol. 7, no. 3, pp. 294–315, 2011.

[95] P. Baptista, J. Conde, J. Rosa, and P. Baptista, “Gold-Nanobeacons as a theranostic system for the detection and inhibition of specific genes,” *Protoc. Exch.*, pp. 1–46, 2013.

[96] Y. Ding *et al.*, “Gold nanoparticles for nucleic acid delivery,” *Mol. Ther.*, vol. 22, no. 6, pp. 1075–1083, 2014.

[97] S. Pelengaris and M. Khan, “The c-MYC oncoprotein as a treatment target in cancer and other disorders of cell growth,” *Expert Opin. Ther. Targets*, vol. 7, no. 5, pp. 623–642, 2003.

[98] M. Vita and M. Henriksson, “The Myc oncoprotein as a therapeutic target for human cancer,” *Semin. Cancer Biol.*, vol. 16, no. 4, pp. 318–330, 2006.

[99] D. M. Miller, S. D. Thomas, A. Islam, D. Muench, and K. Sedoris, “c-Myc and cancer metabolism,” *Clin. Cancer Res.*, vol. 18, no. 20, pp. 5546–5553, 2012.

[100] C. V. Dang, “MYC on the path to cancer,” *Cell*, vol. 149, no. 1, pp. 22–35, 2012.

[101] C. V. Dang, A. Le, and P. Gao, “MYC-induced cancer cell energy metabolism and therapeutic opportunities,” *Clin. Cancer Res.*, vol. 15, no. 21, pp. 6479–6483, 2009.

[102] L. Soucek *et al.*, “Modelling Myc inhibition as a cancer therapy,” *Nature*, vol. 455, no. 7213, pp. 679–683, 2008.

[103] P. C. Lee and D. Meisel, “Adsorption and surface-enhanced Raman of dyes on silver and gold sols,” *J. Phys. Chem.*, vol. 86, no. 17, pp. 3391–3395, Aug. 1982.

[104] T. T. Ahner, F. Delissen, and S. Sokolov, “Mechanism of Gold Nanoparticle Formation in the Classical Citrate Synthesis Method Derived from Coupled In Situ XANES and SAXS Evaluation,” no. 9, pp. 1296–1301, 2010.

[105] M. Uz, V. Bulmus, and S. Alsoy Altinkaya, “Effect of PEG Grafting Density and Hydrodynamic Volume on Gold Nanoparticle–Cell Interactions: An Investigation on Cell Cycle, Apoptosis, and DNA Damage,” *Langmuir*, vol. 32, no. 23, pp. 5997–6009, Jun. 2016.

[106] J. Manson, D. Kumar, B. J. Meenan, and D. Dixon, “Polyethylene glycol functionalized gold nanoparticles: the influence of capping density on stability in various media,” *Gold Bull.*, vol. 44, no. 2, pp. 99–105, 2011.

[107] P. W. Riddles, R. L. Blakeley, and B. Zerner, “Ellman’s reagent: 5,5′-dithiobis(2-nitrobenzoic acid)—a reexamination,” *Anal. Biochem.*, vol. 94, no. 1, pp. 75–81, 1979.

[108] W. Haiss, N. T. K. Thanh, J. Aveyard, and D. G. Fernig, “Determination of Size and Concentration of Gold Nanoparticles from UV−Vis Spectra,” *Anal. Chem.*, vol. 79, no. 11, pp. 4215–4221, Jun. 2007.

[109] Y. Chen *et al.*, "Determination of Size and Concentration of Gold Nanoparticles from UV-Vis Spectra," *Biomaterials*, vol. 34, no. 3, pp. 10217–10227, 2014.

[110] S. Bhattacharjee, "DLS and zeta potential - What they are and what they are not?," *J. Control. Release*, vol. 235, pp. 337–351, 2016.

[111] S. Du, K. Kendall, P. Toloueinia, Y. Mehrabadi, G. Gupta, and J. Newton, "Aggregation and adhesion of gold nanoparticles in phosphate buffered saline," *J. Nanoparticle Res.*, vol. 14, no. 3, p. 758, 2012.

[112] R. Pamies, J. G. H. Cifre, V. F. Espín, M. Collado-González, F. G. D. Baños, and J. G. de la Torre, "Aggregation behaviour of gold nanoparticles in saline aqueous media," *J. Nanoparticle Res.*, vol. 16, no. 4, p. 2376, 2014.

[113] R. Mendes, P. Pedrosa, J. C. Lima, A. R. Fernandes, and P. V Baptista, "Photothermal enhancement of chemotherapy in breast cancer by visible irradiation of Gold Nanoparticles.," *Sci. Rep.*, vol. 7, no. 1, pp. 1–9, 2017.

[114] J. Zhou, J. Ralston, R. Sedev, and D. A. Beattie, "Functionalized gold nanoparticles: Synthesis, structure and colloid stability," *J. Colloid Interface Sci.*, vol. 331, no. 2, pp. 251–262, 2009.

[115] M. Yoshihara, T. Hiyama, and S. Tanaka, "Epidemiology of colorectal cancer," *Nihon Naika Gakkai Zasshi.*, vol. 96, no. 2, pp. 200–206, 2007.

[116] A. Rajput *et al.*, "Characterization of HCT116 Human Colon Cancer Cells in an Orthotopic Model," *J. Surg. Res.*, vol. 147, pp. 276–281, 2008.

[117] W. Strober, "Trypan blue exclusion test of cell viability.," *Curr. Protoc. Immunol.*, vol. 21, no. 1, p. Appendix 3B, May 2001.

[118] S. Kamiloglu, G. Sari, T. Ozdal, and E. Capanoglu, "Guidelines for cell viability assays," *Food Front.*, vol. 1, no. 3, pp. 332–349, Sep. 2020.

[119] M. L. Wong and J. F. Medrano, "Real-time PCR for mRNA quantitation.," *Biotechniques*, vol. 39, no. 1, pp. 75–85, Jul. 2005.

[120] C. F. Dos Santos, V. T. Sakai, M. A. de A. M. Machado, D. N. Schippers, and A. S. Greene, "Reverse transcription and polymerase chain reaction: principles and applications in dentistry.," *J. Appl. Oral Sci.*, vol. 12, no. 1, pp. 1–11, 2004.

[121] T. D. Schmittgen and K. J. Livak, "Analyzing real-time PCR data by the comparative CT method," *Nat. Protoc.*, vol. 3, no. 6, pp. 1101–1108, 2008.

[122] V. Amendola and M. Meneghetti, "Size Evaluation of Gold Nanoparticles by UV−vis Spectroscopy," *J. Phys. Chem. C*, vol. 113, no. 11, pp. 4277–4285, 2009.

[123] K. Jiang, D. A. Smith, and A. Pinchuk, "Size-dependent photothermal conversion efficiencies of plasmonically heated gold nanoparticles," *J. Phys. Chem. C*, vol. 117, no. 51, pp. 27073–27080, 2013.

[124] E. H. M. Sakho, E. Allahyari, O. Oluwafemi, S. Thomas, and N. Kalarikkal, "Dynamic Light Scattering (DLS)," in *Thermal and Rheological Measurement Techniques for Nanomaterials Characterization*, Elsevier, pp. 37–49, 2017.

[125] M. Zimbone *et al.*, "Dynamic Light Scattering on Bioconjugated Laser Generated Gold Nanoparticles," *PLoS One*, vol. 9, no. 3, pp. 1–6, 2014.

[126] M. Danaei *et al.*, “Impact of Particle Size and Polydispersity Index on the Clinical Applications of Lipidic Nanocarrier Systems.,” *Pharmaceutics*, vol. 10, no. 2, pp. 1–17, 2018.

[127] H. Chugh, D. Sood, I. Chandra, V. Tomar, G. Dhawan, and R. Chandra, “Role of gold and silver nanoparticles in cancer nano-medicine,” *Artif. Cells, Nanomedicine Biotechnol.*, vol. 46, no. 1, pp. 1210–1220, 2018.

[128] A. S. Shaik, A. P. Shaik, V. K. Bammidi, and A. Al Faraj, “Effect of polyethylene glycol surface charge functionalization of SWCNT on the in vitro and in vivo nanotoxicity and biodistribution monitored noninvasively using MRI.,” *Toxicol. Mech. Methods*, vol. 29, no. 4, pp. 233–243, 2019.

[129] K. Xiao *et al.*, “The effect of surface charge on in vivo biodistribution of PEG-oligocholic acid based micellar nanoparticles,” *Biomaterials*, vol. 32, no. 13, pp. 3435–3446, 2011.

[130] L. M. Rossi, J. L. Fiorio, M. A. S. Garcia, and C. P. Ferraz, “The role and fate of capping ligands in colloidally prepared metal nanoparticle catalysts,” *Dalt. Trans.*, vol. 47, no. 17, pp. 5889–5915, 2018.

[131] D. Chang *et al.*, “Biologically Targeted Magnetic Hyperthermia: Potential and Limitations.,” *Front. Pharmacol.*, vol. 9, no. 8, p. 831, 2018.

[132] H. J. Kuhn, S. E. Braslavsky, and R. Schmidt, “Chemical actinometry (IUPAC technical report),” *Pure Appl. Chem.*, vol. 76, no. 12, pp. 2105–2146, 2004.

[133] P. Pedrosa, R. Mendes, R. Cabral, L. M. D. R. S. Martins, P. V. Baptista, and A. R. Fernandes, “Combination of chemotherapy and Au-nanoparticle photothermy in the visible light to tackle doxorubicin resistance in cancer cells,” *Sci. Rep.*, vol. 8, no. 1, pp. 1–8, 2018.

[134] M. Kim, J.-H. Lee, and J.-M. Nam, “Plasmonic Photothermal Nanoparticles for Biomedical Applications,” *Adv. Sci.*, vol. 6, no. 17, pp. 1–23, 2019.

[135] J. R. G. Navarro and M. H. V Werts, “Resonant light scattering spectroscopy of gold, silver and gold-silver alloy nanoparticles and optical detection in microfluidic channels.,” *Analyst*, vol. 138, no. 2, pp. 583–592, Jan. 2013.

[136] S. Kumar Panigrahi and A. Kumar Mishra, “Inner filter effect in fluorescence spectroscopy: As a problem and as a solution,” *J. Photochem. Photobiol. C Photochem. Rev.*, vol. 41, pp. 1–28, 2019.

[137] V. Raji, J. Kumar, C. S. Rejiya, M. Vibin, V. N. Shenoi, and A. Abraham, “Selective photothermal efficiency of citrate capped gold nanoparticles for destruction of cancer cells,” *Exp. Cell Res.*, vol. 317, no. 14, pp. 2052–2058, 2011.

[138] E. Spyratou, M. Makropoulou, E. P. Efstathopoulos, A. G. Georgakilas, and L. Sihver, “Recent Advances in Cancer Therapy Based on Dual Mode Gold Nanoparticles,” *Cancers (Basel).*, vol. 9, no. 12, p. 173, Dec. 2017.

[139] H. Norouzi, K. Khoshgard, and F. Akbarzadeh, “In vitro outlook of gold nanoparticles in photo-thermal therapy: a literature review.,” *Lasers Med. Sci.*, vol. 33, no. 4, pp. 917–926, 2018.

[140] X. Huang *et al.*, “Comparative study of photothermolysis of cancer cells with

nuclear-targeted or cytoplasm-targeted gold nanospheres: continuous wave or pulsed lasers.," *J. Biomed. Opt.*, vol. 15, no. 5, p. 1-7, 2010.

[141] C. Yao, F. Rudnitzki, G. Hüttmann, Z. Zhang, and R. Rahmanzadeh, "Important factors for cell-membrane permeabilization by gold nanoparticles activated by nanosecond-laser irradiation.," *Int. J. Nanomedicine*, vol. 12, pp. 5659–5672, 2017.

[142] X. Sun, G. Zhang, R. S. Keynton, M. G. O'Toole, D. Patel, and A. M. Gobin, "Enhanced drug delivery via hyperthermal membrane disruption using targeted gold nanoparticles with PEGylated Protein-G as a cofactor," *Nanomedicine Nanotechnology, Biol. Med.*, vol. 9, no. 8, pp. 1214–1222, 2013.

[143] M. Kodiha, Y. M. Wang, E. Hutter, D. Maysinger, and U. Stochaj, "Off to the organelles - killing cancer cells with targeted gold nanoparticles.," *Theranostics*, vol. 5, no. 4, pp. 357–370, 2015.

[144] V. Amendola, R. Pilot, M. Frasconi, O. M. Maragò, and M. A. Iatì, "Surface plasmon resonance in gold nanoparticles: a review," *J. Phys. Condens. Matter*, vol. 29, no. 20, p. 1-49, 2017.

[145] V. Mulens-Arias, A. Balfourier, A. Nicolás-Boluda, F. Carn, and F. Gazeau, "Endocytosis-driven gold nanoparticle fractal rearrangement in cells and its influence on photothermal conversion," *Nanoscale*, vol. 12, no. 42, pp. 21832–21849, 2020.

[146] B. Kepsutlu *et al.*, "Cells Undergo Major Changes in the Quantity of Cytoplasmic Organelles after Uptake of Gold Nanoparticles with Biologically Relevant Surface Coatings," *ACS Nano*, vol. 14, no. 2, pp. 2248–2264, Feb. 2020.

[147] M. Wang and M. Thanou, "Targeting nanoparticles to cancer," *Pharmacol. Res.*, vol. 62, no. 2, pp. 90–99, 2010.

[148] T. Mantso *et al.*, "Hyperthermia induces therapeutic effectiveness and potentiates adjuvant therapy with non-targeted and targeted drugs in an in vitro model of human malignant melanoma," *Sci. Rep.*, vol. 8, no. 1, pp. 1–16, 2018.

[149] A. N. Daniels and M. Singh, "Sterically stabilized siRNA:gold nanocomplexes enhance c-MYC silencing in a breast cancer cell model," *Nanomedicine*, vol. 14, no. 11, pp. 1387–1401, 2019.

[150] J. Conde *et al.*, "Design of multifunctional gold nanoparticles for in vitro and in vivo gene silencing," *ACS Nano*, vol. 6, no. 9, pp. 8316–8324, 2012.

[151] D. Heinemann *et al.*, "Gold Nanoparticle Mediated Laser Transfection for Efficient siRNA Mediated Gene Knock Down," *PLoS One*, vol. 8, no. 3, p. 1-9, 2013.

[152] R. S. Riley and E. S. Day, "Gold nanoparticle-mediated photothermal therapy: applications and opportunities for multimodal cancer treatment," *WIREs Nanomedicine and Nanobiotechnology*, vol. 9, no. 4, p. 1-16, 2017.

[153] P. J. Goodhew, "General Introduction to Transmission Electron Microscopy TEM," *Aberration-Corrected Anal. Transm. Electron Microsc.*, pp. 1–19, 2011.

[154] P. Foroozandeh and A. A. Aziz, "Insight into Cellular Uptake and Intracellular

Trafficking of Nanoparticles," *Nanoscale Res. Lett.*, vol. 13, pp. 1-12, 2018.

[155] Z. Luo, K. Zheng, Q. Fan, X. Jiang, and D. Xiong, "Hyperthermia exposure induces apoptosis and inhibits proliferation in HCT116 cells by upregulating miR-34a and causing transcriptional activation of p53," *Exp Ther Med*, vol. 14, no. 6, pp. 5379–5386, 2017.

# Annex A

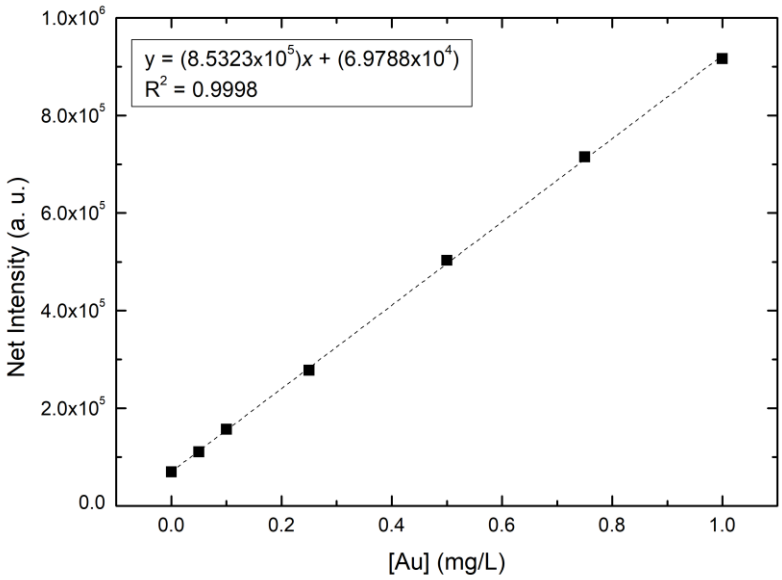


Figure 6.1: Calibration curve for quantification of Au, through ICP-AES.

# Annex B

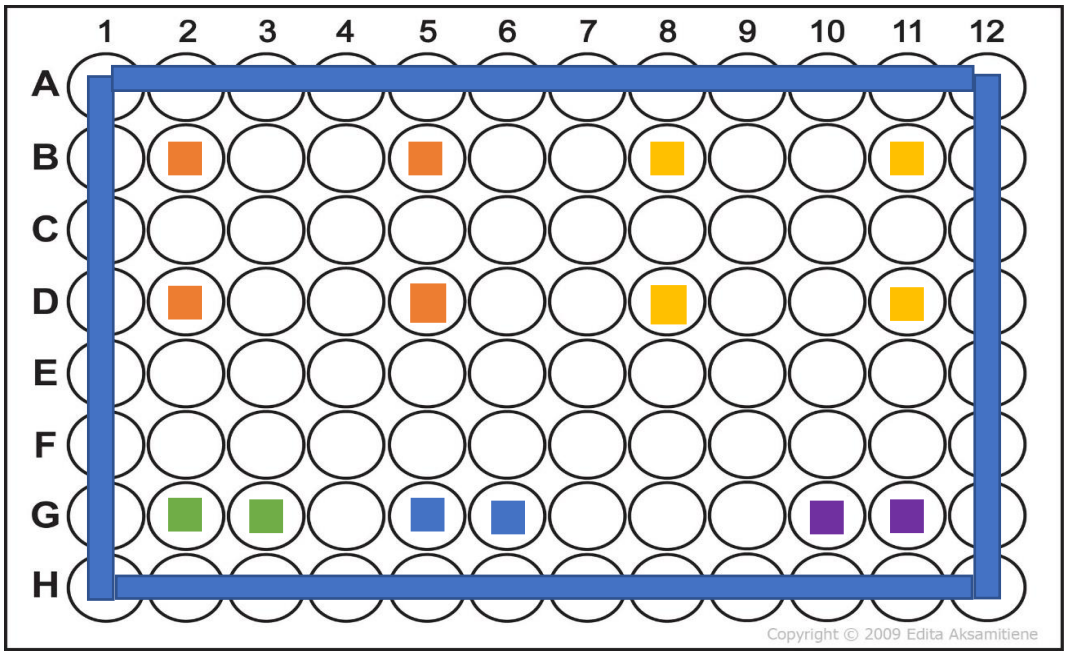


Figure 6.2: Schematic representation of the 96 well plates and the position of each sample: orange represents the cells irradiated with AuNP; yellow cells irradiated; blue the cells with AuNP; purple MTS with the medium; green cells HCT116 cells without AuNPs and laser irradiation.

# Annex C

Table 6.1: Ratio of absorbance (A520/A720) to analyse the level of aggregation of the AuNP in PBS along the time.

| Time (min) | $A_{520}/A_{750}$ |
|---|---|
| 0 | 2.54 |
| 5 | 1.49 |
| 10 | 1.32 |
| 20 | 1.18 |
| 30 | 1.11 |
| 60 | 1.03 |
| 90 | 0.98 |
| 120 | 0.92 |

# Annex D

The Ellman´s assay was performed to analyse if there were any thiols in solution, to indicate the degree of PEG coverage. This colorimetric method is used to quantify the thiol ligands, since DTNB reacts with a free sulfhydryl groups in solution changing the absorbance and colour of the solution. The result of the Ellman´s assay is a calibration curve with several concentrations of PEG, used to apply it into the sample to quantify the thiols in solution. The functionalization of the AuNP was made by adding PEG in excess in the solution. The AuNP@100%PEG had an absorbance of 0.115 and by converting this value to PEG concentration the result is 0 mg/ml, indicating that the PEG added had been successfully functionalize in the surface of the AuNP. For the AuNP@30%PEG the calculated concentration of PEG was 0.000232 mg/ml. This concentration value was approached to zero since it was lower than the limit detection of the calibration curve.

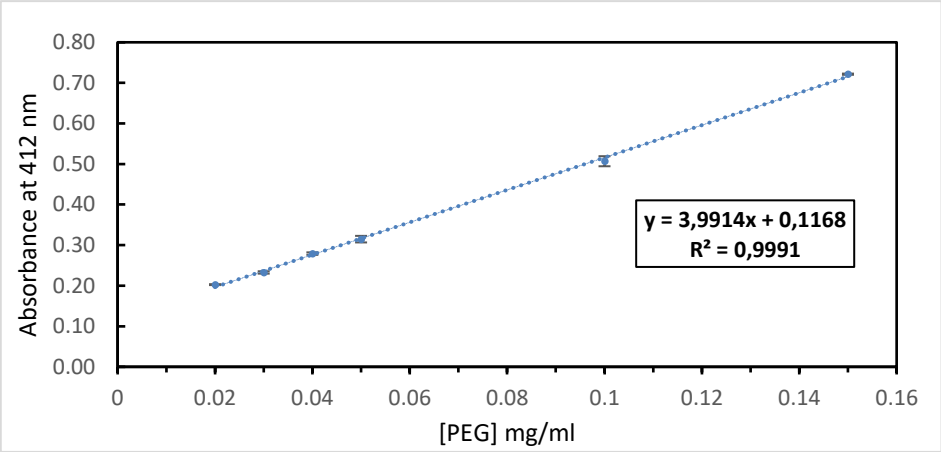


Figure 6.3: Ellman´s calibration curve. The Ellman´s calibration curve was performed to calculate, with the previous standardized solutions, the number of free thiols free in solution that is correlated to the %PEG that is functionalized with the AuNP.

# Annex E

The statistical analysis was made using the GraphPad Prism 6.0 (GraphPad Software, Inc). ANOVA, which stands for Analysis of Variance, is a statistical test used to analyse the difference between the means of more than two groups. The One-way ANOVA test is uses one independent variable, to determine if there is a statistically significant difference between the corresponding population means. Tukey method is a single-step multiple comparison procedure and statistical test. It can be used to find means that are significantly different from each other.

In the following table it is demonstrated the One-way ANOVA test using the Tukey method for the cell viability and the gene expression results.

Table 6.2: One-Way ANOVA test with the cell viability results (for the Trypan Blue) of the variables tested, compared to the control HCT116 cells.

| Tukey´s multiple comparisons test | Mean Diff. | 95.0% CI of diff. | Significant? |
|---|---|---|---|
| HCT116 vs AuNP@PEG | 2.000 | 0.05857 to 3.941 | Yes |
| HCT116 vs Laser | 5.000 | 3.059 to 6.941 | Yes |
| HCT116 vs AuNP@Laser | 9.000 | 7.059 to 10.94 | Yes |

Table 6.3: One-Way ANOVA test with the cell viability results (for the MTS) of the variables tested, compared to the control HCT116 cells.

| Tukey´s multiple comparisons test | Mean Diff. | 95.0% CI of diff. | Significant? |
|---|---|---|---|
| HCT116 vs AuNP@PEG | 0.1352 | -0.07825 to 0.3486 | No |
| HCT116 vs Laser | 0.2003 | -0.01315 to 0.4137 | No |
| HCT116 vs AuNP@Laser | 0.2279 | 0.01440 to 0.4413 | Yes |

Table 6.3: One-Way ANOVA test with the cell viability results (for the combinatory approach between gene silencing and phototherapy) of the variables tested, compared to the control HCT116 cells.

| Tukey´s multiple comparisons test | Mean Diff. | 95.0% CI of diff. | Significant? |
|---|---|---|---|
| HCT116 vs AuNP@MYC | 0.2021 | 0.120436 to 1.09216 | No |
| HCT116 vs AuNP@MYC@Laser | 0.3020 | 0.8853 to 0.5154 | Yes |

Table 6.3: One-Way ANOVA test with gene expression results of the variables tested, compared to the control AuNP@PEG.

| Tukey´s multiple comparisons test | Mean Diff. | 95.0% CI of diff. | Significant? |
|---|---|---|---|
| HCT116 vs AuNP@MYC | 0.606297 | 0.120436 to 1.09216 | Yes |
| HCT116 vs AuNP@MYC@Laser | 0.820105 | 0.334244 to 1.30597 | Yes |